SRNL-TR-2009-00041

Key Words:
Assimilation
Radar

Retention:
#Permanent#

ASSIMILATION OF DOPPLER RADAR DATA INTO NUMERICAL WEATHER MODELS

Co-author: Steven R. Chiswell
Co-author: Robert L. Buckley

JANUARY 31, 2009

Savannah River National Laboratory
Savannah River Nuclear Solutions
Aiken, SC 29808
Prepared for the U.S. Department of Energy Under Contract Number DE-AC09-08SR22470

DISCLAIMER

Printed in the United States of America

Prepared for
U.S. Department of Energy

SRNL-TR-2009-00041

Key Words:
Assimilation
Radar

Retention:
#Permanent#

ASSIMILATION OF DOPPLER RADAR DATA INTO NUMERICAL WEATHER MODELS

Co-author: Steven R. Chiswell
Co-author: Robert L. Buckley

JANUARY 31, 2009

Savannah River National Laboratory
Savannah River Nuclear Solutions
Savannah River Site
Aiken, SC 29808

Prepared for the U.S. Department of Energy Under
Contract Number DE-AC09-08SR22470

REVIEWS AND APPROVALS

Steven R. Chiswell, Co-author, Atmospheric Technologies Group Date

Robert L. Buckley, Co-author, Atmospheric Technologies Group Date

Lance O'Steen, Technical Reviewer, Atmospheric Technologies Group Date

Charles H. Hunter, Level 4 Manager, Atmospheric Technologies Group Date

Robert P. Addis, Level 3 Manager, National and Homeland Security Date

TABLE OF CONTENTS

LIST OF FIGURES ..... **iv**
LIST OF ACRONYMS ..... **v**
1.0 EXECUTIVE SUMMARY **1**
2.0 INTRODUCTION **2**
3.0 DOPPLER RADAR ASSIMILATION **4**
4.0 CASE STUDY OF AUGUST 4, 2008 ..... **6**
4.1 Synoptic Analysis of the Storm Environment **7**
4.2 Model Analysis **11**
4.3 Application to Atmospheric Transport **18**
5.0 CONCLUSIONS **20**
6.0 REFERENCES **22**
7.0 APPENDIX A. Infrared Satellite Images August 3-4, 2008 ..... **24**
8.0 APPENDIX B. Radar Images 23:04-23:59 UTC August 03, 2008 ..... **33**
9.0 APPENDIX C. Locations of SRS Meteorological Towers **40**

LIST OF FIGURES

Figure 1. Comparison of *legacy* 1.0 km (top) and *super resolution* 0.25 km resolution (bottom) for Columbia, SC at 00 UTC August 4, 2008. 3

Figure 2. As in Fig 1, except root mean squared difference field computed for assimilation after QC processing. 5

Figure 3. Columbia, SC three-dimensional *super resolution* radar reflectivity display depicting thunderstorm development at 2359 UTC August 3, 2008 as viewed from the southeast as depicted in Figs. 1 & 2. 6

Figure 4. Surface analysis for 0000 UTC August 4, 2008 (sea level pressure (mb) yellow lines, surface fronts and weather features, and Convective Available Potential Energy (CAPE)) from 12km NAM. 8

Figure 5. Columbia, SC radar display for 2355 UTC, Aug 3, 2008. The cold air outflow boundary identified from radar animation is indicated by the white line (Bottom). 9

Figure 6. Temperature (degrees C) recorded at meteorological towers within SRS during the period 1200 UTC Aug 3 to 0600 UTC Aug 4, 2008. The temperature drop in response to thunderstorm activity between 2245 UTC and 0115 UTC is most pronounced at towers P and L and decreases northward and westward from these locations. See Appendix C for individual tower locations. 10

Figure 7. As in Figure 5, with the 0000 UTC Aug 4, 2008 NCEP operational NAM 12km 2 m temperature analysis (magenta lines) shown. The model analysis shows that cold pools generated by thunderstorm outflow in the vicinity of surface observing stations (shown in yellow) are present in the model initialization. 11

Figure 8. Model comparison for base case (Top) and radar case (bottom) showing 2m temperature field (degrees C) and 10m streamlines (yellow lines) for 0030 UTC. 12

Figure 9. As in figure 8, but for 0200 UTC. 14

Figure 10a. Model simulated radar reflectivity (shaded areas) and wind streamlines for base case (top) and radar case (bottom) for 0045 UTC. 15

Figure 10b. Model simulated radar reflectivity (shaded areas) and wind streamlines for base case (top) and radar case (bottom) for 0115 UTC. 16

Figure 11. Wind direction from SRS observations (brown), base run (blue) and radar initialized run (yellow) for 0100-0600 UTC. A subset of towers is shown for clarity. 18

Figure 12. HYSPLIT runs for base case (left) and radar assimilation case (right) depicting concentrations at 45 minutes (top) and 4 hours (bottom) for a simulated release within SRS. 19

Figure 13. Observed radar reflectivity (Top) viewed from NW at 0000 UTC Aug 4, 2008. Model forecast cloud water (yellow), ice (orange), and precipitation (blue) isosurfaces at 0045 UTC (bottom). Note the model domain is a subset of the radar image domain. 21

LIST OF ACRONYMS

3DVAR	Three-Dimensional Variational data assimilation
CAPE	Convective Available Potential Energy
HYSPLIT	Hybrid Single-Particle Lagrangian Integrated Trajectory
KCAE	Columbia, SC National Weather Service Radar Identifier
LDRD	Laboratory Directed Research and Development
NAM	North American Mesoscale
NCEP	National Centers for Environmental Prediction
NEXRAD	Next Generation Radar
NWS	National Weather Service
QC	Quality Control
SRS	Savannah River Site
UTC	Universal Time Coordinated
WRF	Weather Research and Forecasting Model
WSR-88D	Weather Service Radar (NEXRAD generation 1988)

1.0 EXECUTIVE SUMMARY

During the year 2008, the United States National Weather Service (NWS) completed an eight fold increase in sampling capability for weather radars to 250 m resolution. This increase is expected to improve warning lead times by detecting small scale features sooner with increased reliability; however, current NWS operational model domains utilize grid spacing an order of magnitude larger than the radar data resolution, and therefore the added resolution of radar data is not fully exploited. The assimilation of radar reflectivity and velocity data into high resolution numerical weather model forecasts where grid spacing is comparable to the radar data resolution was investigated under a Laboratory Directed Research and Development (LDRD) "quick hit" grant to determine the impact of improved data resolution on model predictions with specific initial proof of concept application to daily Savannah River Site operations and emergency response.

Development of software to process NWS radar reflectivity and radial velocity data was undertaken for assimilation of observations into numerical models. Data values within the radar data volume undergo automated quality control (QC) analysis routines developed in support of this project to eliminate empty / missing data points, decrease anomalous propagation values, and determine error thresholds by utilizing the calculated variances among data values. The Weather Research and Forecasting model (WRF) three dimensional variational data assimilation package (WRF-3DVAR) was used to incorporate the QC'ed radar data into input and boundary conditions.

The lack of observational data in the vicinity of SRS available to NWS operational models signifies an important data void where radar observations can provide significant input. These observations greatly enhance the knowledge of storm structures and the environmental conditions which influence their development. As the increase in computational power and availability has made higher resolution real-time model simulations possible, the need to obtain observations to both initialize numerical models and verify their output has become increasingly important. The assimilation of high resolution radar observations therefore provides a vital component in the development and utility of numerical model forecasts for both weather forecasting and contaminant transport, including future opportunities to improve wet deposition computations explicitly.

2.0 INTRODUCTION

The ability to accurately specify the initial state of the atmosphere is critical in order for numerical weather models to produce useful results. *In situ* observations are the most common source of knowledge of model initial conditions; although the spatial resolution of regularly available data is generally less than the resolution of current operational weather models and the observations themselves contain inherent uncertainty and limitations. The initial period of model integration needed for physical processes to reproduce and sustain the conditions representing the original set of discrete sampled observations is referred to as the model spin-up time, and generally requires several hours of model integration. During the model spin-up period, the ability of the model to outperform simple extrapolation of initial conditions is often limited (Lin *et al*., 2005). Doppler weather radars provide the ability to remotely sample three-dimensional storm structures through measurements of reflectivity, velocity and returned power spectra. Assimilation of radar velocity and precipitation fields into high-resolution model simulations can improve precipitation forecasts with decreased "spin-up" time and improve short-term simulation of boundary layer winds (Benjamin *et al.*, 2004, 2007 & 2009; Xiao *et al*., 2008) which is critical to improving transport forecasts for airborn contaminants. Accurate description of wind and turbulence fields is essential to useful atmospheric transport and dispersion results, and any improvement in the accuracy of these fields will make consequence assessment more valuable to decision makers during emergency situations.

During 2008, the United States National Weather Service (NWS) implemented a significant upgrade to the operational radar network which increased the real-time level II data resolution to 8 times their previous “legacy” resolution, from 1 km range gate and 1.0 degree azimuthal resolution to “super resolution” 250 m range gate and 0.5 degree azimuthal resolution (Fig 1). These radar observations provide reflectivity, velocity and returned power spectra measurements at a range of up to 300 km (460 km for reflectivity) at a frequency of 4-5 minutes and yield up to 13.5 million point observations per level in super-resolution mode. The migration of National Weather Service (NWS) WSR-88D radars to *super resolution* is expected to improve warning lead times by detecting small scale features sooner with increased reliability; however, current operational mesoscale model domains utilize grid spacing several times larger than even the *legacy* data resolution. Therefore the added resolution of radar data is not fully exploited in model “spin-up”, placing a greater dependency on parameterization schemes for sub-grid scale cumulus physics.

The assimilation of *super resolution* reflectivity and velocity data into high resolution numerical weather model forecasts where grid spacing is comparable to the radar data resolution is investigated here to determine the impact of the improved data resolution on storm scale model predictions. A case study is performed in order to develop a methodology toward implementing radar assimilation in an operational setting.

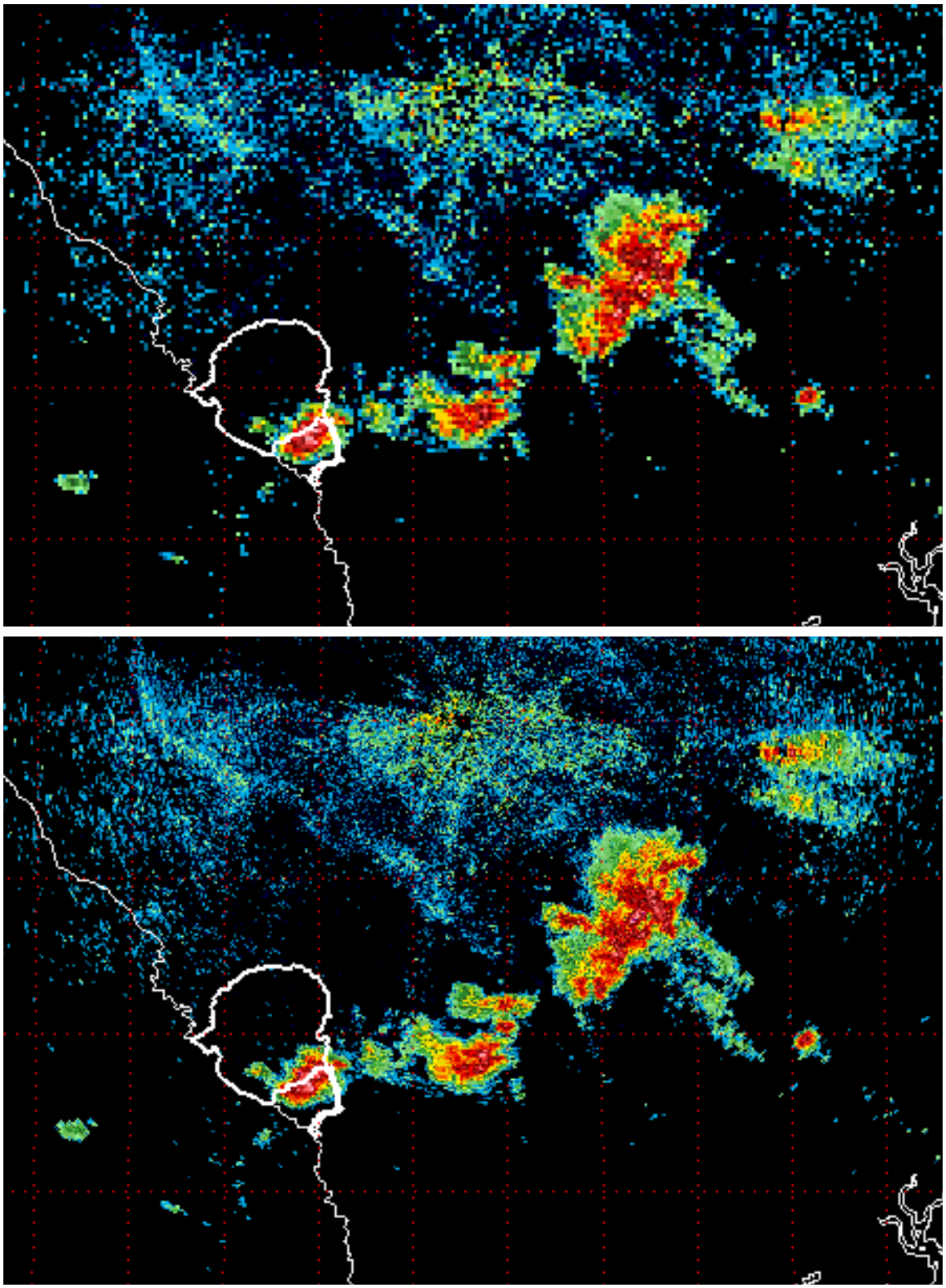

Figure 1. Comparison of *legacy* 1.0 km (top) and *super resolution* 0.25 km resolution (bottom) for Columbia, SC at 00 UTC August 4, 2008.

3.0 DOPPLER RADAR ASSIMILATION

The physical processes leading to precipitation within numerical weather prediction models must include a balance of diabatic heating as well as dynamic and thermal response in order to maintain numerical stability. Attempts to nudge precipitation within models using precipitation measurements, previous model forecasts, or radar/satellite estimates have often been problematic in maintaining convection and/or generating spurious precipitation, generating non-physical motion, or conserving quantities of heat, moisture and radiation within parameterized convection schemes. The availability of high resolution three-dimensional Doppler radar fields provides a significant source of storm scale measurements which allow for integration with explicit calculation of precipitation physics while providing sufficient resolution for resolving grid scale features which would otherwise receive little weight in assimilation routines.

Development of software to process NWS Level II radar reflectivity and radial velocity data was undertaken for automated assimilation of real-time or archived observations into numerical models. In order to prepare the radar observations, a coordinate transformation is performed to convert the radial coordinate data into a volumetric cube. Values are extracted at each point within the cube where data undergo quality control (QC) analysis to eliminate empty / missing data points, decrease anomalous propagation values, and determine error thresholds by calculating 9-point variances utilizing adjacent row and column data values for all points. Ground clutter contamination was suppressed through simultaneous comparison of reflectivity and velocity fields, and requiring zero velocity areas to exceed 3 km vertical extent and 20 dBZ maximum column reflectivity (FMH-11, Part B, 2005, Guo *et al.*, 2005). By comparison to *legacy* resolution, it is clear that the use of *super resolution* data decreases the variance of the radar fields as there is less difference among adjacent data points (Fig 2) which leads to an overall improvement in assimilation weighting. The Weather Research and Forecasting model (WRF) three dimensional variational data assimilation package (WRF-3DVAR) (Barker *et al*., 2004) was used to incorporate the *super resolution* data into the WRF input and boundary conditions by formatting the processed radar profiles into vertical point observations (Xiao *et al*., 2008). For the Level II Doppler radar data (three-dimensional radial velocity and reflectivity), WRF-3DVAR utilities for Richarson's equation and water hydrometeor analysis achieve balance with physical and microphysical model quantities. Direct assimilation of radar data is accomplished through WRF-3DVAR by minimizing the difference between data observations and their model observation operator counterparts without the need to transform radar retrievals into separate model variables prior to inclusion.

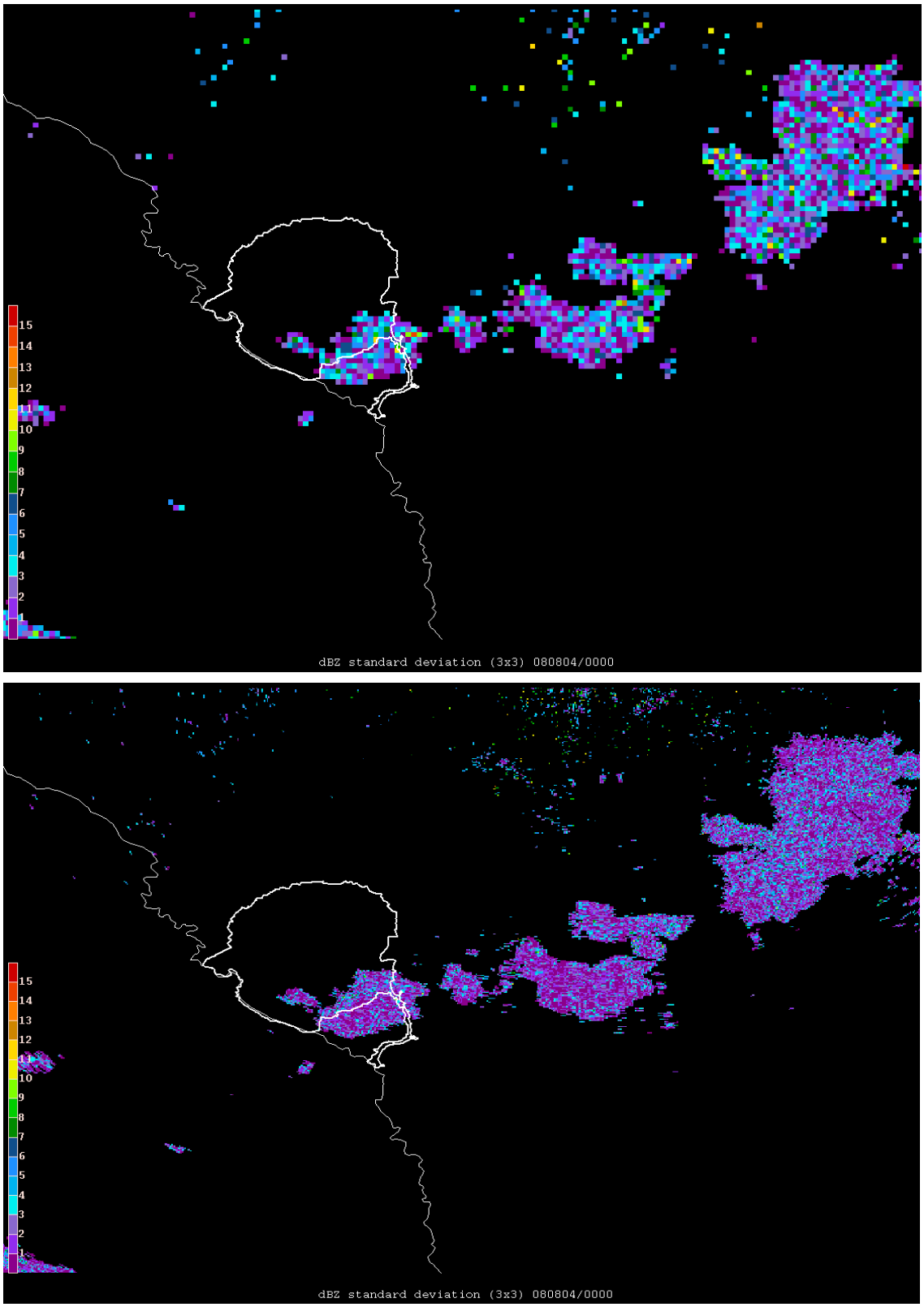

Figure 2. As in Fig 1, except root mean squared difference field computed for assimilation after QC processing.

4.0 CASE STUDY OF AUGUST 4, 2008

A case study was performed to assess the impact and utility of assimilating *super resolution* radar observations, and to develop a methodology for applying the technique for operational use. The Columbia, South Carolina radar location (KCAE) is the closest WSR-88D site in proximity to the Savannah River Site (SRS) and is approximately 91 km (56 mi) NNE of the center of the site. The KCAE radar was upgraded to *super resolution* on July 23, 2008. On the evening of August 3, 2008, shortly after KCAE radar began transmitting *super resolution* observations, a weak, nearly stationary frontal boundary provided a focusing mechanism for late afternoon convection (Fig 3).

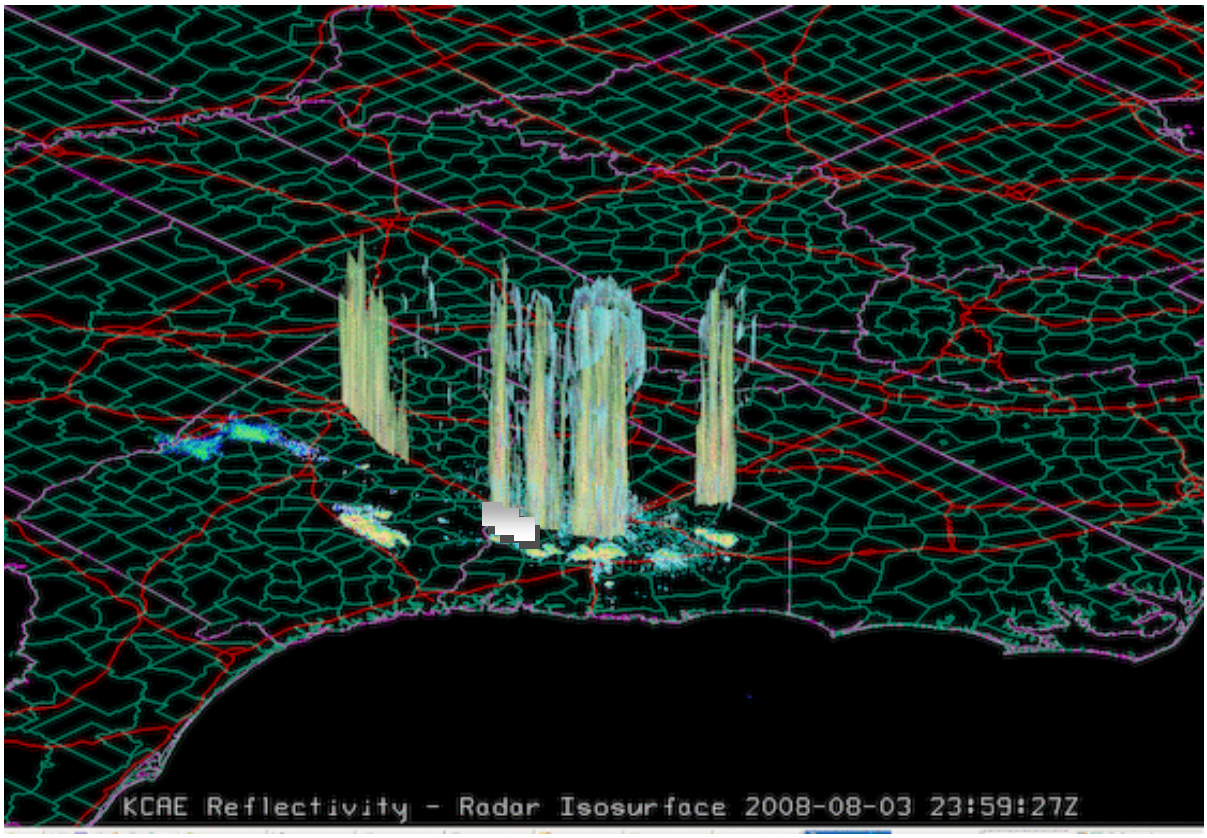

Figure 3. Columbia, SC three-dimensional *super resolution* radar reflectivity display depicting thunderstorm development at 2359 UTC August 3, 2008 as viewed from the southeast as depicted in Figs. 1 & 2.

The time period beginning 00 UTC (Universal Time Coordinated) August 4, 2008 was chosen for a case study since it presented precipitation conditions in and around SRS at the time of the National Center for Environmental Prediction (NCEP) operational model initialization and could highlight the benefit of radar data assimilation. NCEP's operational 12 km resolution North American Mesoscale (NAM) model, which does not incorporate radar data in its analysis, was used to provide the initial and boundary conditions for local higher resolution model runs centered on SRS. A base run utilizing WRF with a 2.5 km outer grid and a 0.5 km interior nest grid provided the control for comparison with a second run utilizing radar data assimilation from KCAE at the time of model initialization. Additional

control runs for 00 UTC and 12 UTC runs for the previous three days (6 runs covering 3 diurnal cycles) were used to generate background error fields for WRF-3DVAR using NCEP's T+24/T+12 method (Barker *et al*., 2004) which utilizes the history of differences in forecasts over subsequent runs to create model error perturbation fields as an estimate of forecast error. Both 00 UTC and12 UTC runs were used to remove diurnal bias in model error estimates. The assimilation of radar data utilized both the reflectivity as well as velocity fields at all beam elevation angles by interpolating the observations to a data cube. The error estimates for assimilation of the radar fields was specified by the root mean square difference of observed radar values in the surrounding 3x3 grid of observations in the cube following the methodology by Xiao *et al*. (2008).

4.1 SYNOPTIC ANALYSIS OF THE STORM ENVIRONMENT

Surface conditions present on August 3-4, 2008 reveal a weak cold front extending south from low pressure off the coast of Maine becoming nearly stationary over South Carolina (SC) and extending westward through Mississippi (Fig 4). High pressure expanding southward from the Great Lakes produced generally clear conditions beneath its dome with scattered convection ringing its periphery. Convective Available Potential Energy (CAPE) values along and ahead of the frontal system were moderately high, ranging from 3250 J/Kg to 4000 J/Kg in the vicinity of the SRS with the frontal boundary providing a focus for low level convergence. Daytime temperatures reached 34 °C (low-90s °F) across SRS, with dewpoint temperatures of 23 °C (low-mid 70s °F) which are typical of summer conditions in the southeast United States. Scattered afternoon thunderstorms had developed across SC and Georgia (GA) the previous day under similar conditions, although developing further to the north and west and dissipating as the storms approached SRS as daytime heating diminished. Thunderstorms formed a third consecutive day in the vicinity of SRS during the evening of August 4, 2008 along the stalled frontal boundary, demonstrating the persistent influence of the feature (See Appendix A for hourly infrared satellite images from 01 UTC Aug 3 through 00 UTC Aug 5, 2008). Moderate vertical wind shear existed both in speed and direction as a result of the frontal zone. Maximum wind speed gusts observed at the SRS climatology site were 19 mph at 4m, and 37 mph at 61m.

Radar imagery from Columbia, SC shows a line of scattered thunderstorms oriented from northeast to southwest and passing through SRS in the hour preceding the 00 UTC, Aug 4, 2008 model initialization (See Appendix B for individual radar images during this period) with several of the storm cells passing through the southern portion of SRS. An animation of the radar images during this period reveals a distinct pattern of thunderstorm cold-air outflow (App. B) extending outward from the storms located to the southeast of the radar site (Fig 5). It should be noted that the outflow pattern is most evident in the immediate vicinity of the radar site where the elevation angle of the radar beam is below the top of the layer of cold air generated by the rain cooled downdraft generated by the precipitating thunderstorms. As the radar beam extends outward from the radar site, the beam increases its elevation above the ground as a result of the curvature of the earth. The absence of outflow signatures at greater distances does not indicate that they are not present, but rather, if present, they are below the elevation angle of the radar beam. Data from meteorological towers within SRS show a temperature drop of up to 8 °C in response to the thunderstorm passing through the site

between 2245 UTC Aug 3 and 0115 UTC Aug 4, 2008 with the P and L towers showing the greatest impact. (Fig 6).

Comparing the location of the cold pool identified by radar (Fig 5) with the NCEP operational 12km North American Mesoscale (NAM) model analysis of 2m temperature for 0000 UTC Aug 4 shows that feature is generally resolved well, and furthermore, that other cold pools generated by thunderstorm outflows in the vicinity of surface observing stations are present in the model initialization as well. However, there is a lack of surface observation sites in the vicinity of SRS that are incorporated into the NCEP operational models, and therefore the cold outflow associated with the storm affecting SRS (as observed in Fig 6) is not reflected in the NCEP analysis.

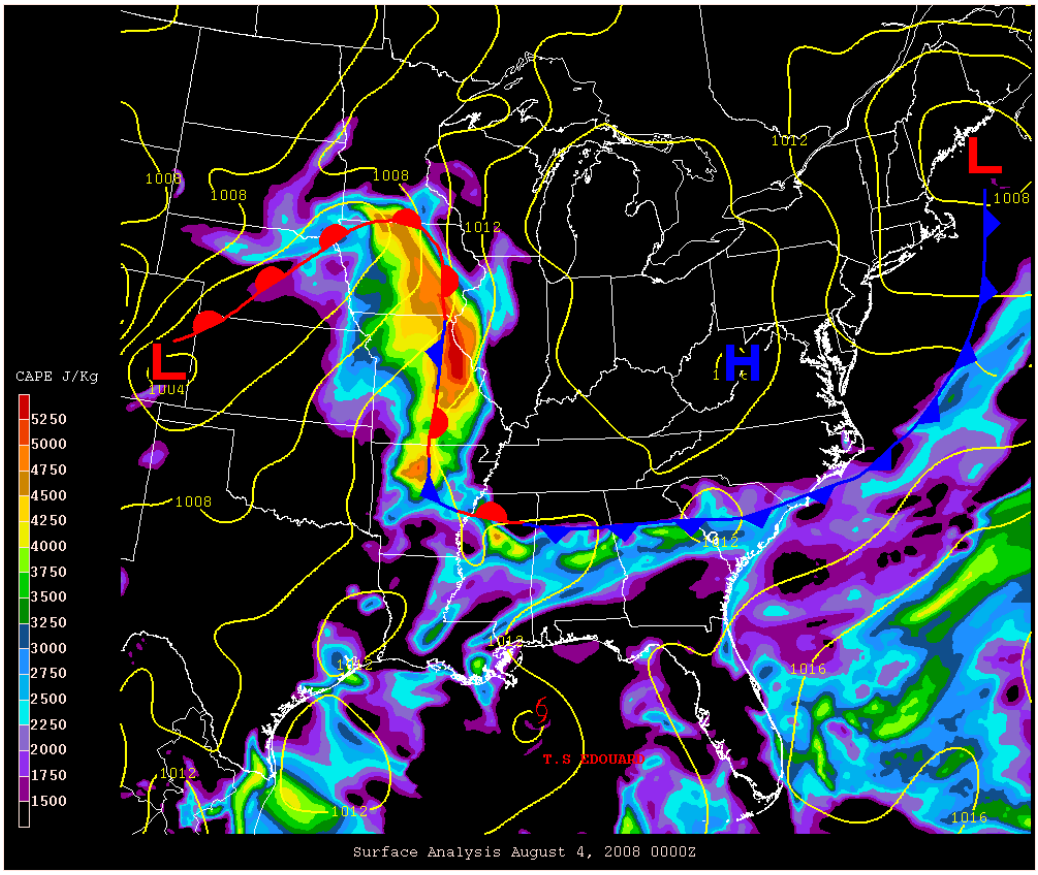

Figure 4. Surface analysis for 0000 UTC August 4, 2008 (sea level pressure (mb) yellow lines, surface fronts and weather features, and Convective Available Potential Energy (CAPE)) from 12km NAM.

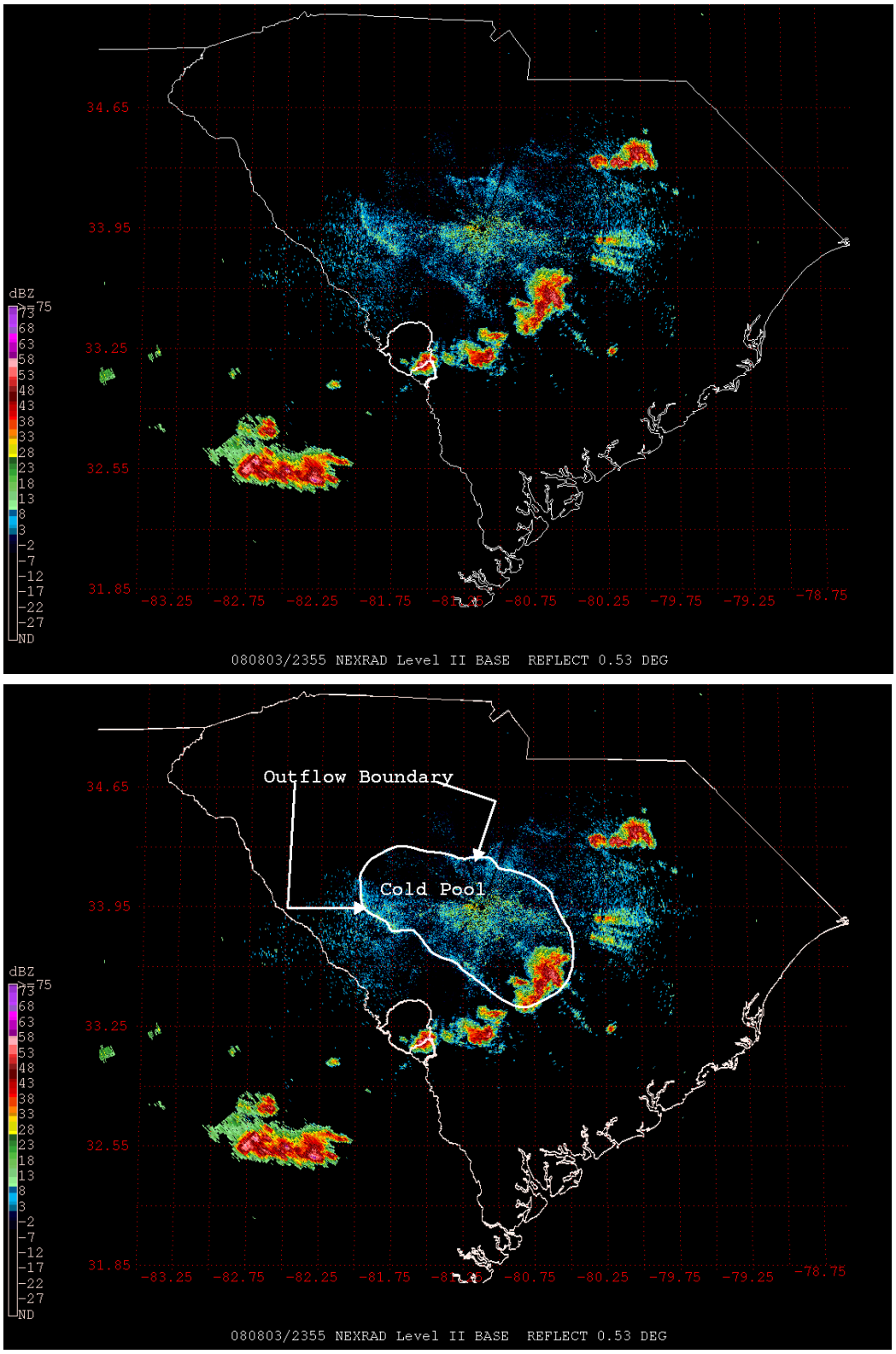

Figure 5. Columbia, SC radar display for 2355 UTC, Aug 3, 2008. The cold air outflow boundary identified from radar animation is indicated by the white line (Bottom).

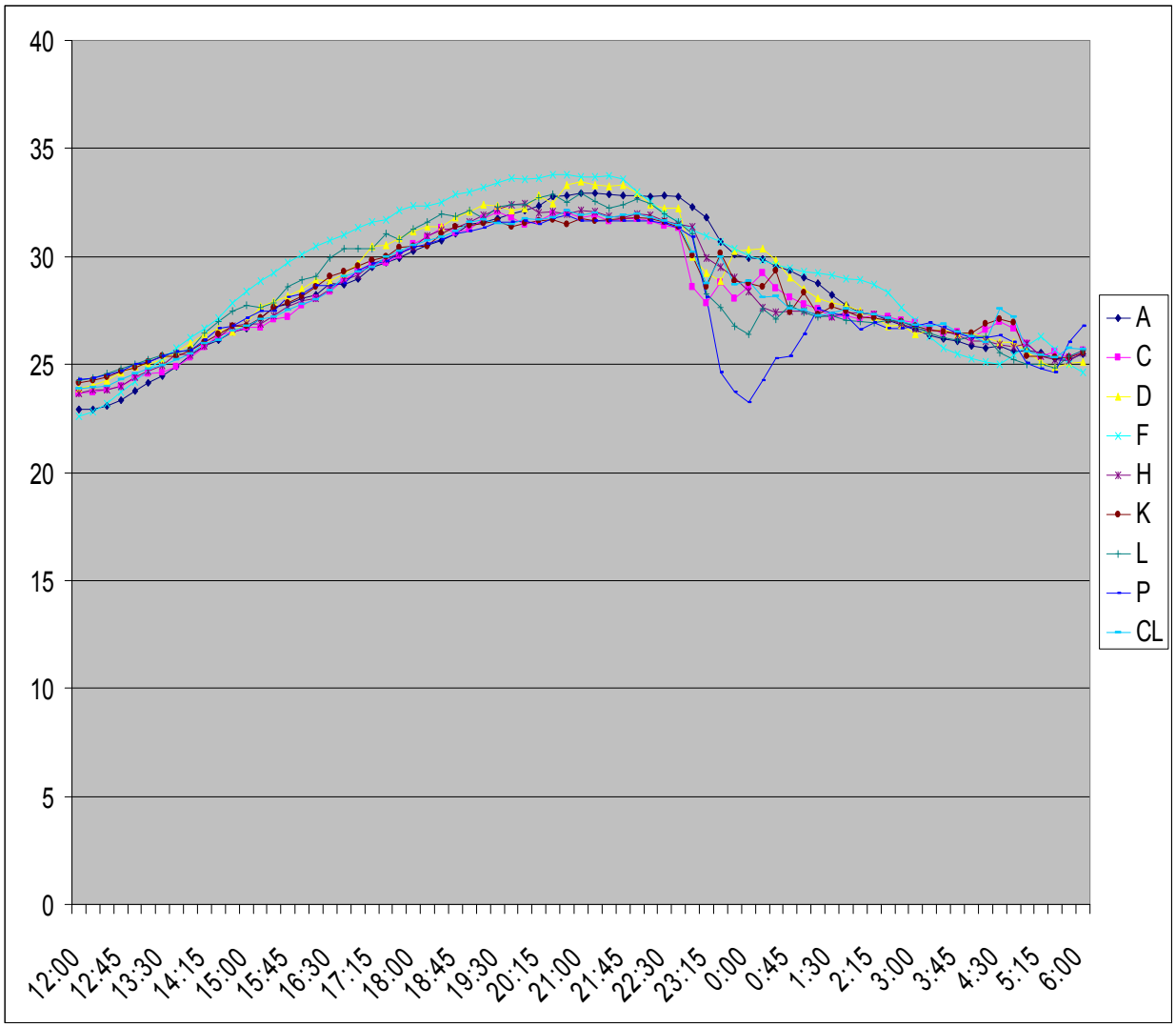

Figure 6. Temperature (degrees C) recorded at meteorological towers within SRS during the period 1200 UTC Aug 3 to 0600 UTC Aug 4, 2008. The temperature drop in response to thunderstorm activity between 2245 UTC and 0115 UTC is most pronounced at towers P and L and decreases northward and westward from these locations. See Appendix C for individual tower locations.

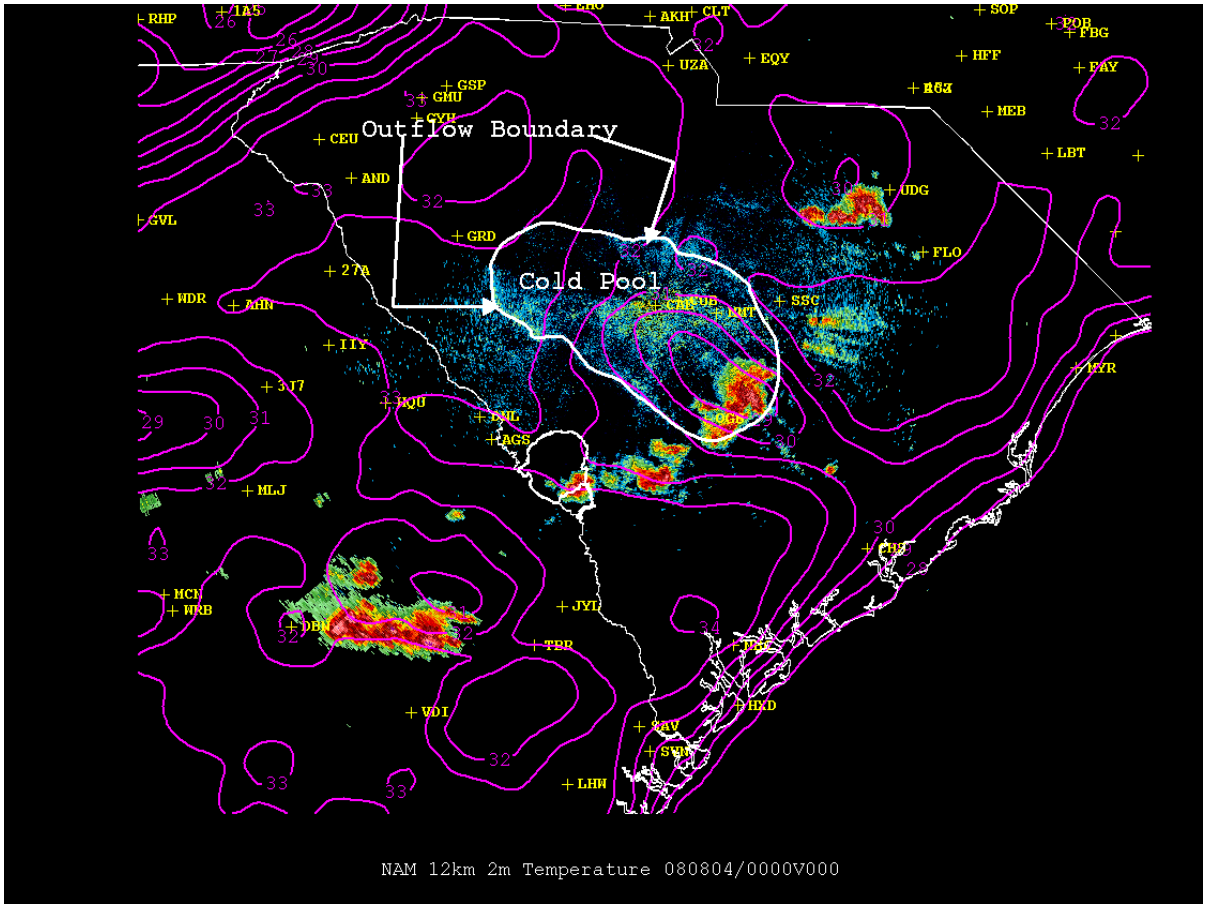

Figure 7. As in Figure 5, with the 0000 UTC Aug 4, 2008 NCEP operational NAM 12km 2 m temperature analysis (magenta lines) shown. The model analysis shows that cold pools generated by thunderstorm outflow in the vicinity of surface observing stations (shown in yellow) are present in the model initialization.

4.2 MODEL ANALYSIS

Utilizing the NCEP 12 km operational NAM model to provide initial and boundary conditions for base case and radar assimilation case runs as described above, a comparison of 15 minute output was performed to assess the impact of radar data on the model forecasts. An immediate consequence of the assimilation of radar data is readily apparent in direct comparison of the base case and radar case, where the adjustment of the wind and temperature fields in response to features discernable in radar images is evident (Fig 8). The temperature and wind fields (10 m streamlines) in the base case clearly reflect the influence of the initially analyzed cold pool which dominates the scene. Alternatively, in addition to the large outflow feature to the northeast of SRS, the radar case demonstrates activity of additional storm cells at 30 minutes iteration, including the thunderstorm located in the southeast portion of SRS. Moreover, the large cold pool outflow no longer poses a singular dominant feature, but rather one of a number of cores of convective activity.

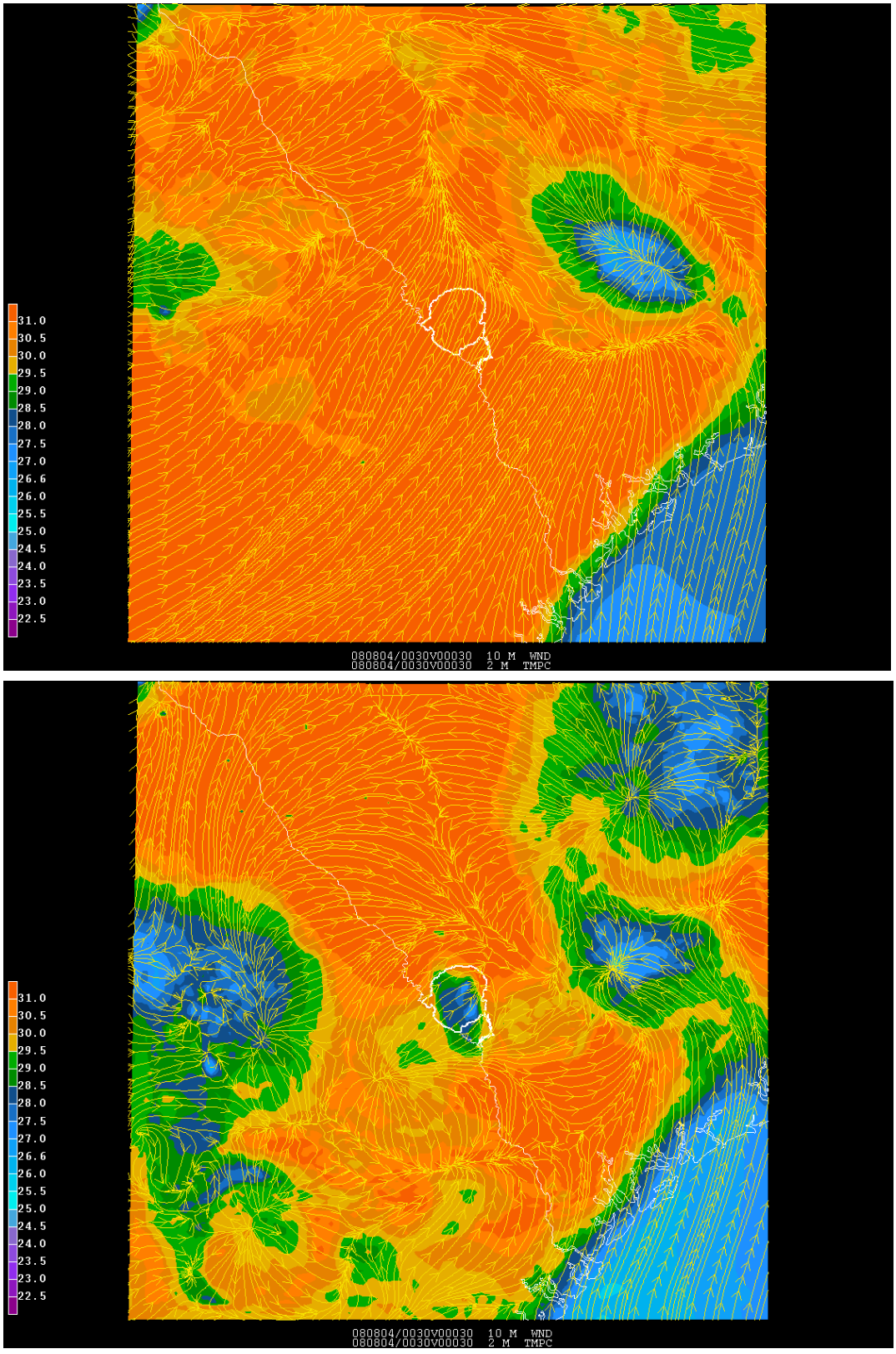

Figure 8. Model comparison for base case (Top) and radar case (bottom) showing 2m temperature field (degrees C) and 10m streamlines (yellow lines) for 0030 UTC.

By two hours into model integration time, the base case evolved into a number of isolated convective cores, while the radar case was exhibiting advanced thunderstorm development. The general lack of convection being developed over SRS in the base case can be attributed to the slower *spin-up* time and the dominant cold pool, such that the observed outflow environment in the initialization acted to suppress convection by expanding in areal coverage prior to the model being able to support convection in this region, thereby stabilizing the environment. Both model runs demonstrate the motion of thunderstorm cells southeastward, while the formation of new cells is propagated northward upstream (a feature confirmed in satellite imagery as in Appendix A), although the propagation in the base case is generally due to the expansion of the existing cold pool boundary, while the radar case shows new generation from independent storm cells (Fig 9). Analysis of the model output shows faster spin up to precipitation when radar data is assimilated. By 45 minutes into the model runs, there is little precipitation in the base case, while there is considerable established convective precipitation in the radar initialized run. Model output from the radar run shows an established thunderstorm cell over eastern and southeastern SRS (Fig 10). The minimum temperature of 23 °C, recorded at tower P during thunderstorm passage, as seen in Figure 6 is accurately depicted in location and magnitude by the radar model forecast as well (see Fig 9). In comparison, the model environment temperature without radar data assimilation is found to remain near 30 °C over most of SRS through 0200 UTC. The 7 °C temperature range evident in SRS tower observations clearly underscores the local effects of thunderstorm outflow, and the ability of radar observations to position the storm locations during model initialization is well illustrated.

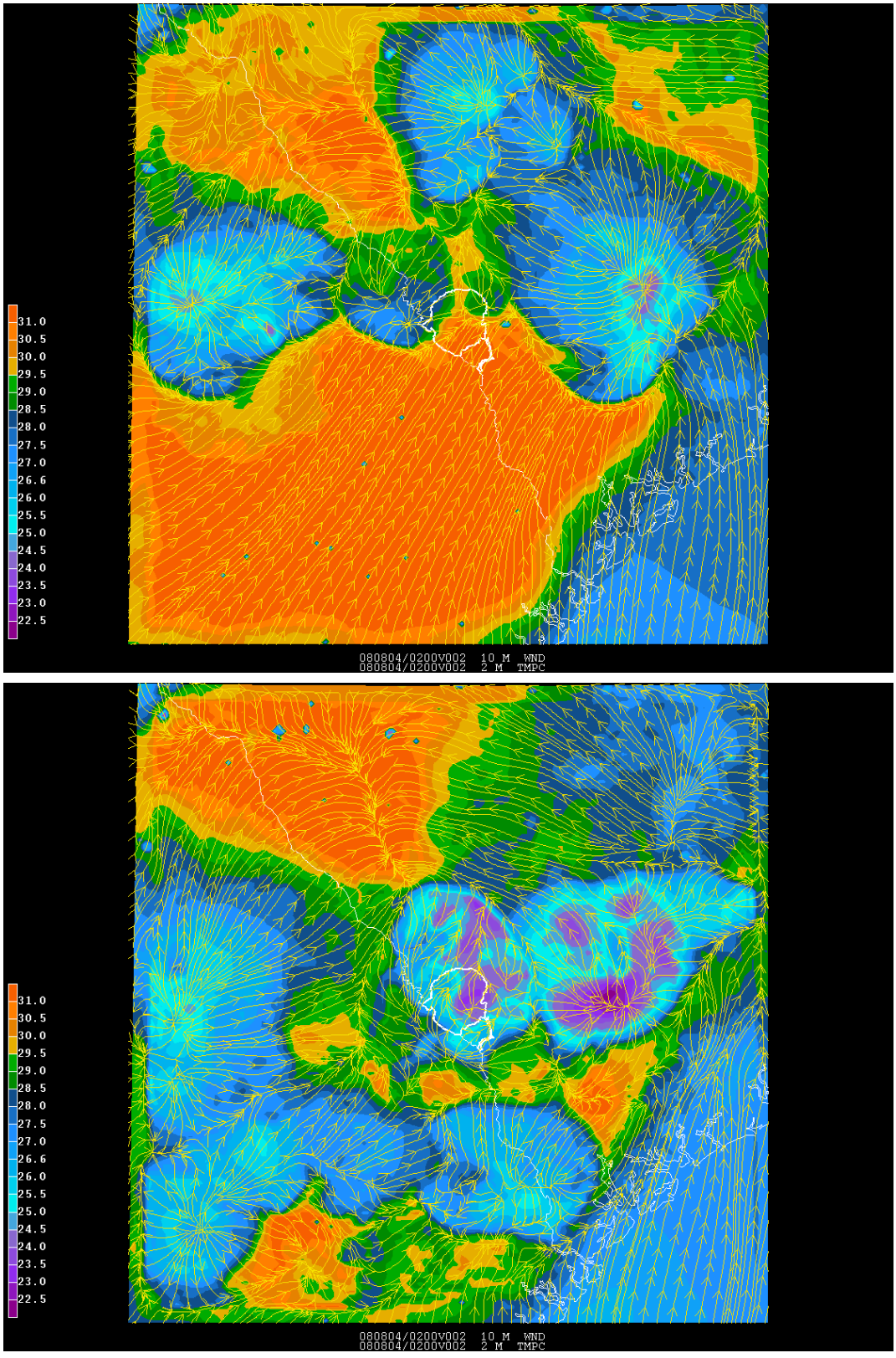

Figure 9. As in figure 8, but for 0200 UTC.

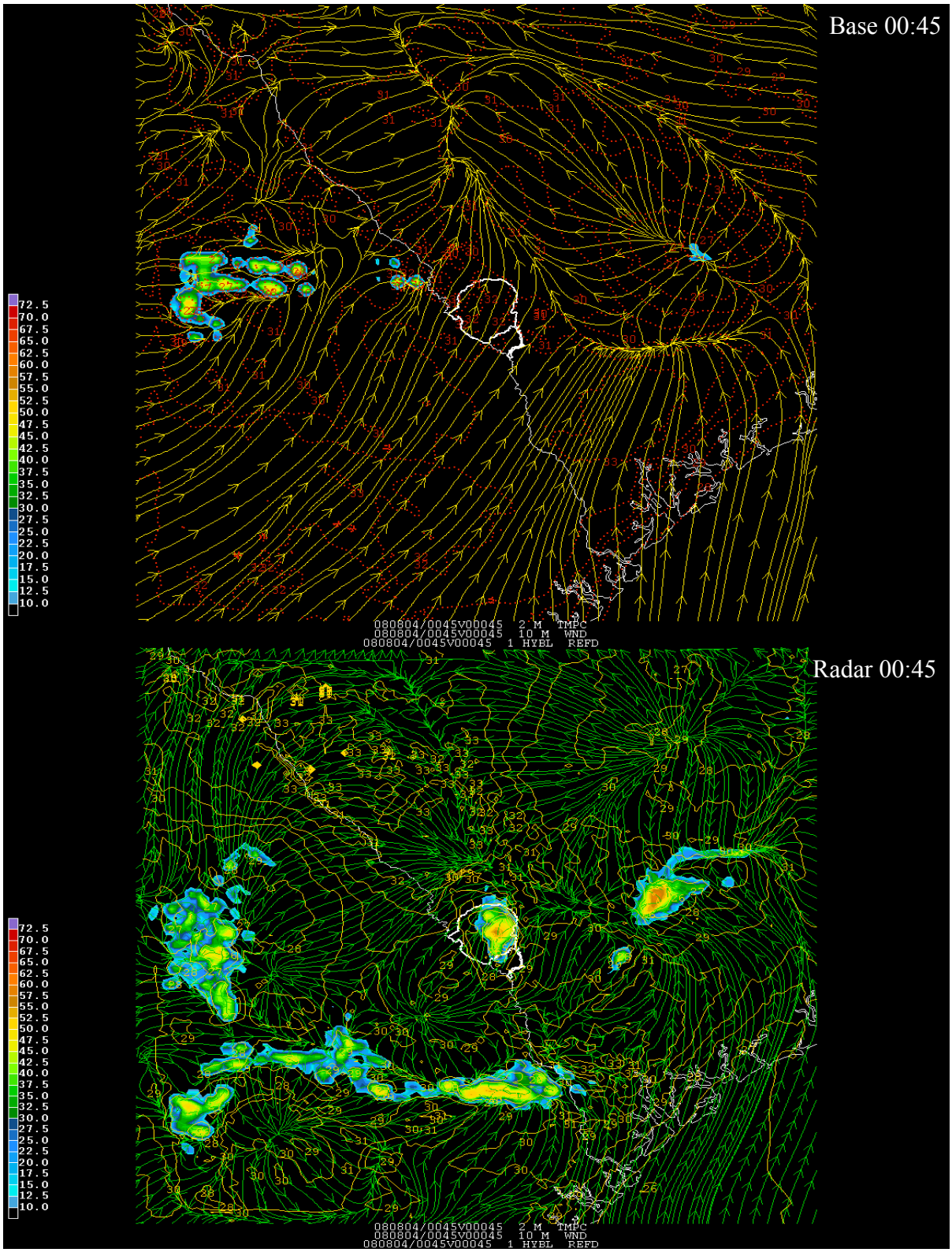

Figure 10a. Model simulated radar reflectivity (shaded areas) and wind streamlines for base case (top) and radar case (bottom) for 0045 UTC.

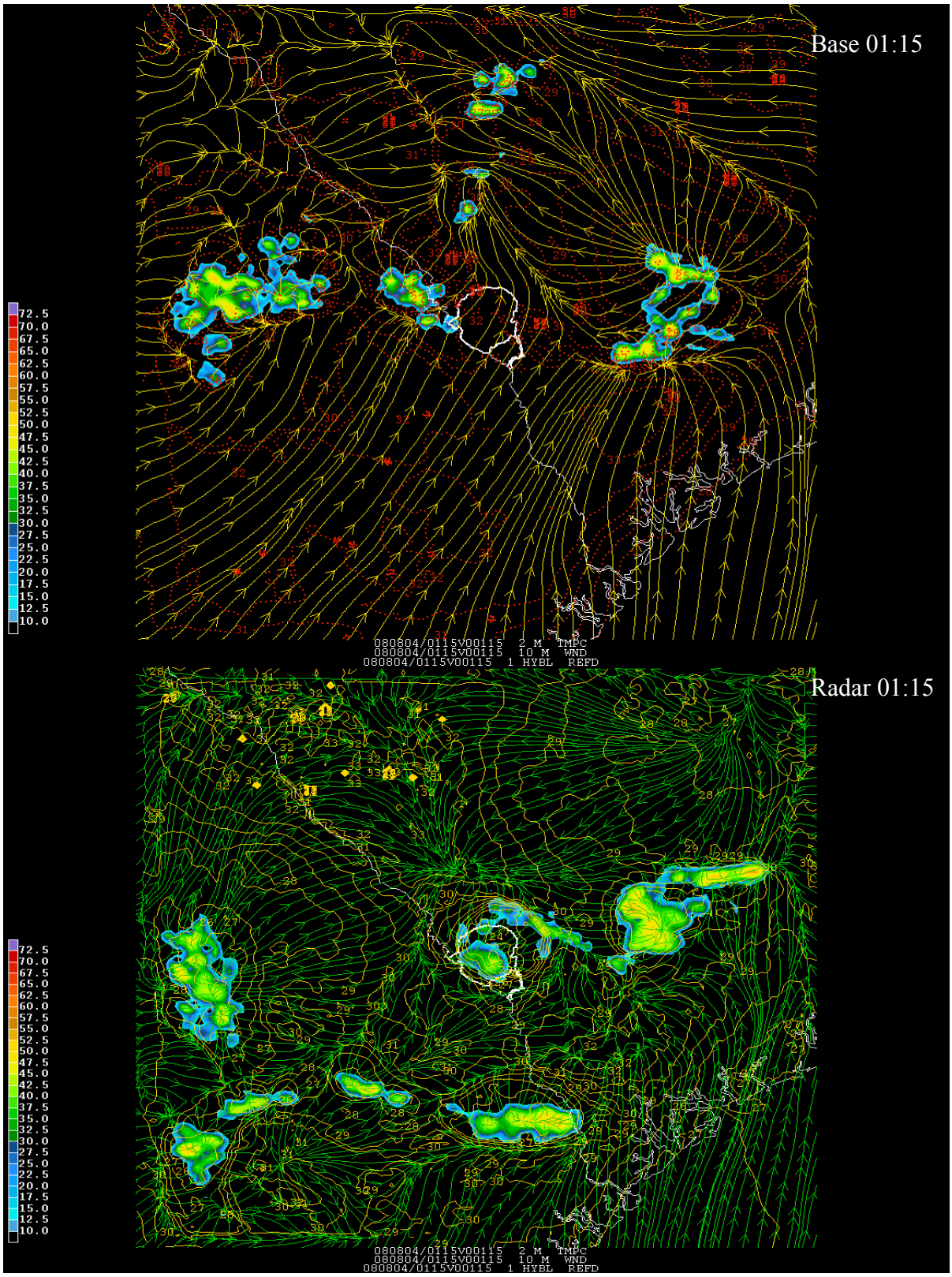

Figure 10b. Model simulated radar reflectivity (shaded areas) and wind streamlines for base case (top) and radar case (bottom) for 0115 UTC.

In order to compare instantaneous model simulated winds with 15 minute observed wind measurements recorded from SRS meteorological towers at a height of 61m, a site average for both 10m above ground level and the lower boundary layer (0 to 30 mb above the surface) was computed from the instantaneous wind fields generated at each output time of the model runs. Comparison of these fields reveal that the radar assimilation run provides a better agreement during the first 6 hours of simulation, after which, both the assimilation and base runs show little difference due to the dissipation of convective activity and a return to weakly driven nighttime flow and diminished effect of the influence of local data assimilation at greater time periods (Fig 11). Model differences in 10m and lower boundary layer site area averaged wind speed and direction are seen to be greatest during storm activity. During periods of storm activity, the boundary layer averaged wind is shown to be more representative of the 61m tower level than the model surface (10m) value as seen in Figure 11 between 0200 UTC to 0330 UTC. Standard deviation of tower wind (sigma-azimuth) direction was between 10-17 degrees for each site location except during periods of storm activity when values exceeding 45 degrees over 15 minutes were found at sites nearest the storm centers. Predicted wind direction for the radar assimilation run, assuming mean boundary layer winds, was found to be within the range of site tower wind direction measurements for the first 3.25 hours of simulation, while the base case direction varied up to 45 degrees from the observations. After this period, both the radar and base case runs show a second line of storm development evident in the wind profiles and which is in agreement with satellite imagery as well. The range of observed wind direction among the SRS towers increases significantly after 0315 UTC due to both local storm conditions initially, and later as a result of generally light ambient winds.

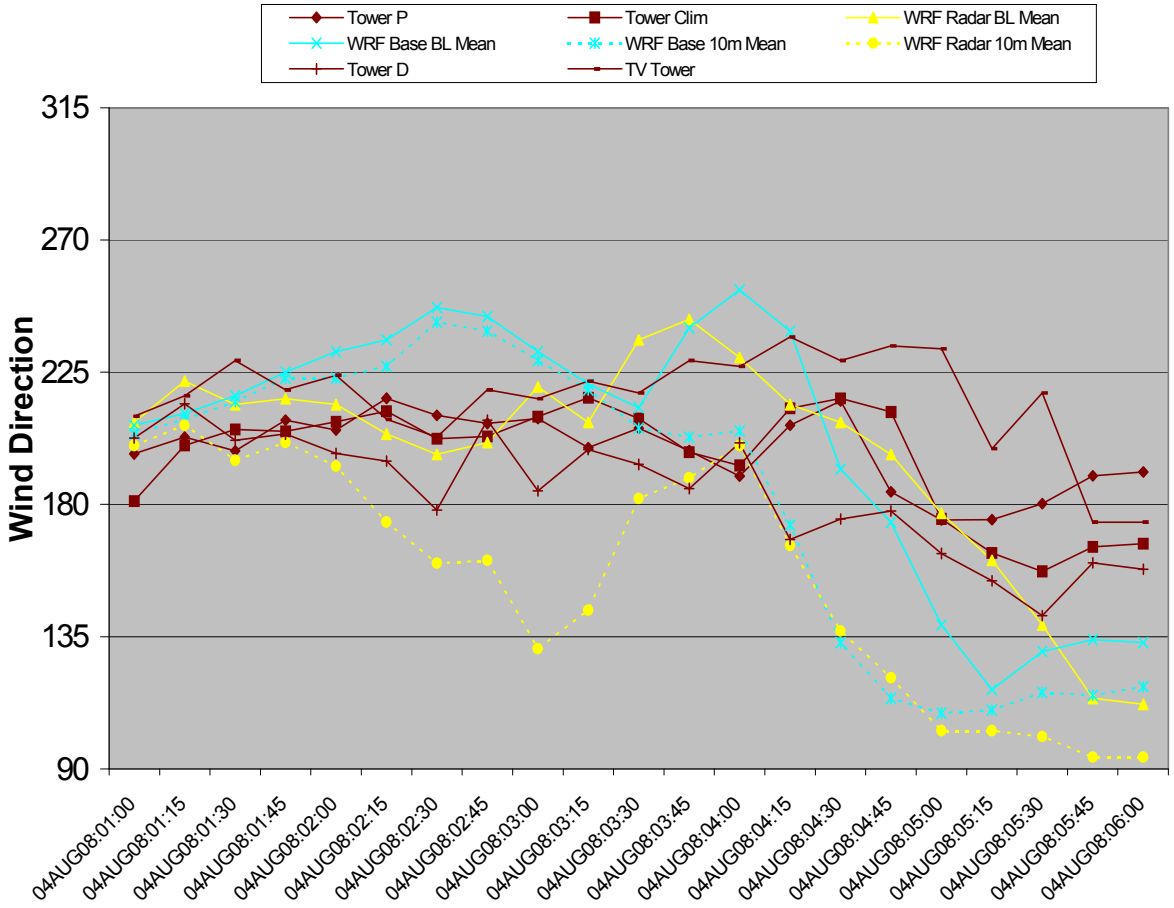

Figure 11. Wind direction from SRS observations (brown), base run (blue) and radar initialized run (yellow) for 0100-0600 UTC. A subset of towers is shown for clarity.

4.3 APPLICATION TO ATMOSPHERIC TRANSPORT

The Hybrid Single-Particle Lagrangian Integrated Trajectory (HYSPLIT) was used to generate atmospheric transport of a hypothetical continuous unit contaminant release (1 Ci hr^{-1}) at an elevation of 10 meters above the ground using forecast wind output for the two model simulations. HYSPLIT has been used in a variety of atmospheric simulation scenarios and has been thoroughly validated against observations (Draxler and Hess, 1997; 1998) and used in a variety of studies (Draxler, 2003; Draxler, 2006; Escudero et al., 2006; and Stein et al., 2007). Turbulence is calculated using the horizontal and vertical velocity variances within the model forecast fields. Surface concentration was calculated assuming effluent within the lowest 50 meters above ground while no removal processes were considered (Fig 12).

The general pattern of both runs is indicative of the larger scale northeasterly transport direction with initial meandering due to the outflow of storms located to the south and west. The primary affect of the generation of convection in the vicinity of SRS prior to 02 UTC in the assimilation case is increased plume spread and slightly lower maximum surface concentrations. The arrival of the cold air pool driven by thunderstorm outflow is seen in

both runs between 03 UTC to 08 UTC as an abrupt shift to winds from the east as the frontal boundary moves south of SRS. By comparison, the radar assimilation case shows a large area of fumigation which spreads over two-thirds of the SRS site area while the base case shows considerably less areal spread (see Fig. 12). The period of rapid fumigation occurs coincident with the period where the 10 m and lower boundary layer model wind directions show the greatest differences. Such differences clearly impact emergency response efforts if an actual release were to have occurred at this time where the radar assimilation case scenario has significant impact to the western half of the SRS, while the base case does not. This example illustrates the importance of accurate wind and turbulence measurement and forecasts in reliable consequence assessment of atmospheric releases. Further investigations including wet deposition removal processes would be a valuable follow up activity as well.

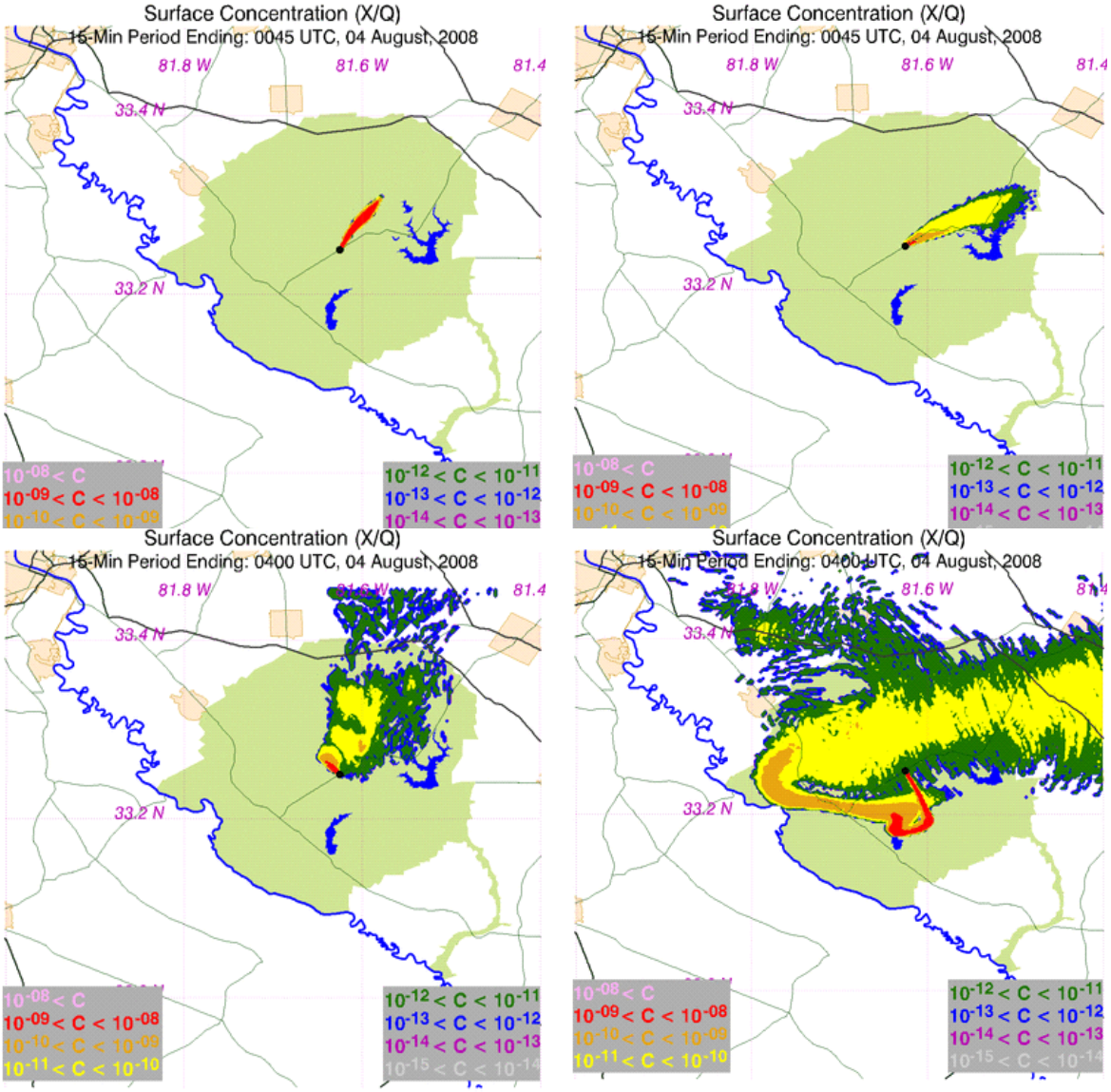

Figure 12. HYSPLIT runs for base case (left) and radar assimilation case (right) depicting concentrations at 45 minutes (top) and 4 hours (bottom) for a simulated release within SRS.

5.0 CONCLUSIONS

The advent of real-time distribution of Level II Doppler radar data provides a wealth of information describing the atmospheric state in and around the storm environment. Within numerical weather prediction models there is a great potential to utilize the information that Doppler radar observations can provide in order to improve the specification of the observational state beyond the capability of traditional observations of model state variables. As the increase in computational power and availability has made higher resolution real-time model simulations possible, the need to obtain observations to both initialize numerical models and verify their output has become increasingly important (Fig 13). Radar observations can provide high temporal and spatial resolution input to models; however, there have been practical limits on the use of high resolution data due to the demands of conducting explicit calculation rather than the parameterization of grid scale processes. The addition of *super resolution* Doppler radar data further enhances the ability to resolve physical processes on the storm scale and significant development has taken place in developing models which can take advantage of these advances.

The lack of observational data in the vicinity of SRS available to NCEP's operational models signifies an important data void where radar observations can provide significant input for both model initialization as well as verification. The assimilation of *super resolution* radar observations therefore provides a vital component in the development and utility of these models. The increase in radar data resolution decreases the root mean squared difference of the assimilated fields thereby improving the contribution of these fields to the model analysis. These observations greatly enhance the specification of initial storm structures and environmental conditions which influence their development. The *spin-up* time for precipitation was observed to be less when radar data was assimilated for the August 4, 2008 case study. The effect of the distribution of turbulent mixing also underscores the benefit that precipitation and three-dimensional wind fields can have on the modeled forecast.

The application of Level II radar observations in a case study enabled an operational methodology to be developed in order to assimilate observations in real-time. The results of this case study illustrated several areas in which radar observations can improve model results. Further application of radar data is also indicated in atmospheric transport models by impacting wet deposition removal processes. A longer period of application will provide a much richer dataset for analysis and development of quality control algorithms necessary to provide the best possible data for assimilation.

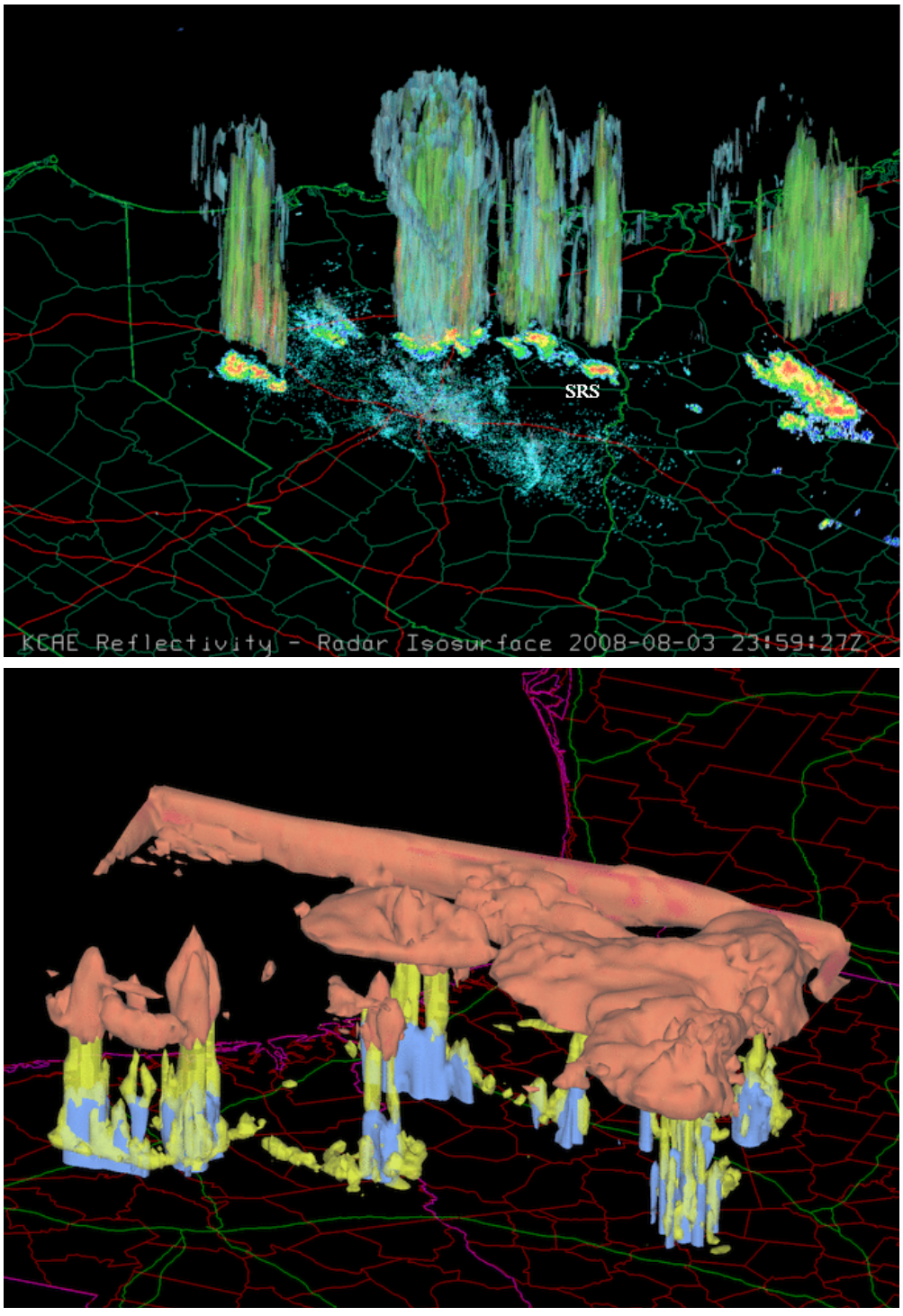

Figure 13. Observed radar reflectivity (Top) viewed from NW at 0000 UTC Aug 4, 2008. Model forecast cloud water (yellow), ice (orange), and precipitation (blue) isosurfaces at 0045 UTC (bottom). Note the model domain is a subset of the radar image domain.

6.0 REFERENCES

Barker, D.M., W. Huang, Y. R. Guo, and Q. N. Xiao., 2004: A Three-Dimensional (3DVAR) Data Assimilation System For Use With MM5: Implementation and Initial Results. *Mon. Wea. Rev*., **132**, 897-914.

Benjamin, S. G., and co-authors, 2004: An hourly assimilation/forecast cycle: the RUC. *Mon. Wea. Rev*., **132**, 495-518.

Benjamin, S. G., and co-authors, 2007: From the radar-enhanced RUC to the WRF-based rapid refresh. *22nd Conf. Wea. Analysis Forecasting/18th Conf. Num. Wea. Pred.*, Park City, UT, Amer. Meteo. Soc., June.

Benjamin, S. G., W. R. Moninger, B. D. Jamison, and S. R. Sahm, 2009: Relative short-range forecast impact in summer and winter from aircraft, profiler, rawinsonde, VAD, GPS-PW, METAR and mesonet observations for hourly assimilation into the RUC. 25th Conf International Information Precessing Systems, Phoenix, AZ. Amer. Meteo. Soc..

Draxler, R.R. and G.D. Hess, 1998: An Overview of the Hysplit_4 Modeling System for Trajectories, Dispersion, and Deposition. *Aust. Met. Mag*., **47**, 295-308.

Draxler, R.R. and G.D. Hess, 1997: Description of the Hysplit_4 modeling system. NOAA Tech Memo ERL ARL-224, 24p.

Draxler, R.R., 2003: Evaluation of an ensemble dispersion calculation. *Journal of Applied Meteorology*, **42**, 308-317.

Draxler, R.R.,2006: The Use of Global and Mesoscale Meteorological Model Data to Predict the Transport and Dispersion of Tracer Plumes over Washington, D.C. *Weather and Forecasting*, **21** (3), 383-394.

Escudero, M., A. Stein, R. R. Draxler, X. Querol, A. Alastuey, S. Castillo, and A. Avila ,2006: Determination of the contribution of northern Africa dust source areas to PM10 concentrations over the central Iberian Peninsula using the Hybrid Single-Particle Lagrangian Integrated Trajectory model (HYSPLIT) model. *J. Geophys. Res*., **111**, D06210, doi:10.1029/2005JD006395.

Federal Meteorological Handbook No. 11, Part B, Doppler Radar Theory and Meteorology (2005), FCM-H11B-2005, http://www.ofcm.gov/fmh11/fmh11B.htm.

Gao, J., K. Brewster, and M. Xue, 2005: Differences Between Explicit and Approximated Radar Ray Paths Due to the Vertical Gradient of Refractivity. 32nd Conf. Radar Meteorology.

Lin, C.A., S. Vasić, A. Kilambi, B. Turner and I. Zawadzki, 2005: Precipitation forecast skill of numerical weather prediction models and radar nowcasts. Geophys. Res. Lett. 32, L14801.

Stein, A.F., V. Isakov, J. Godowitch, R.R. Draxler, 2007: A hybrid modeling approach to resolve pollutant concentrations in an urban area. *Atmospheric Environment,* **41**, 9410-9426.

Xiao, Q., and co-authors, 2008: Doppler radar data assimilation in KMA's operational forecasting. *Bull. Amer. Meteor. Soc*., **89** (1), 39-43.

7.0 APPENDIX A. INFRARED SATELLITE IMAGES AUGUST 3-4, 2008

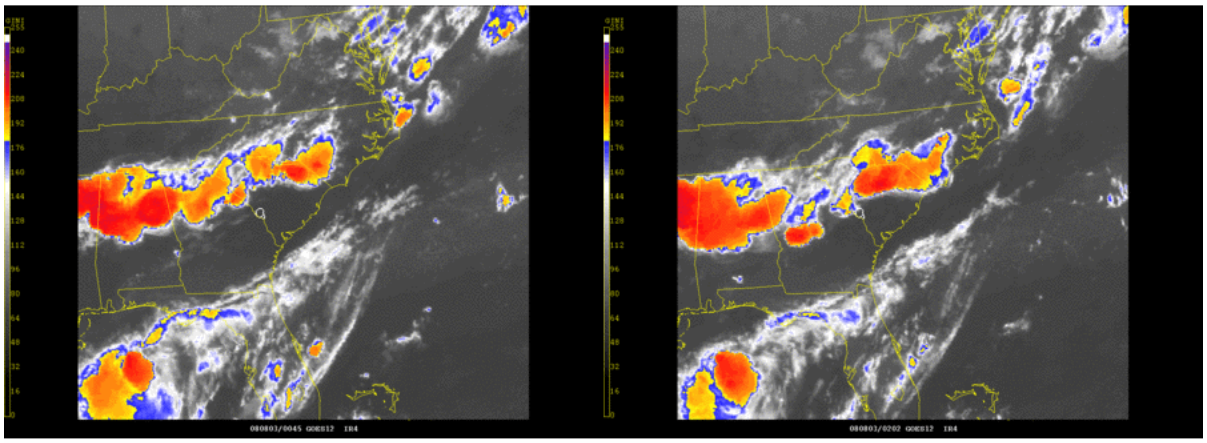

Aug 3, 2008 01Z

Aug 3, 2008 02Z

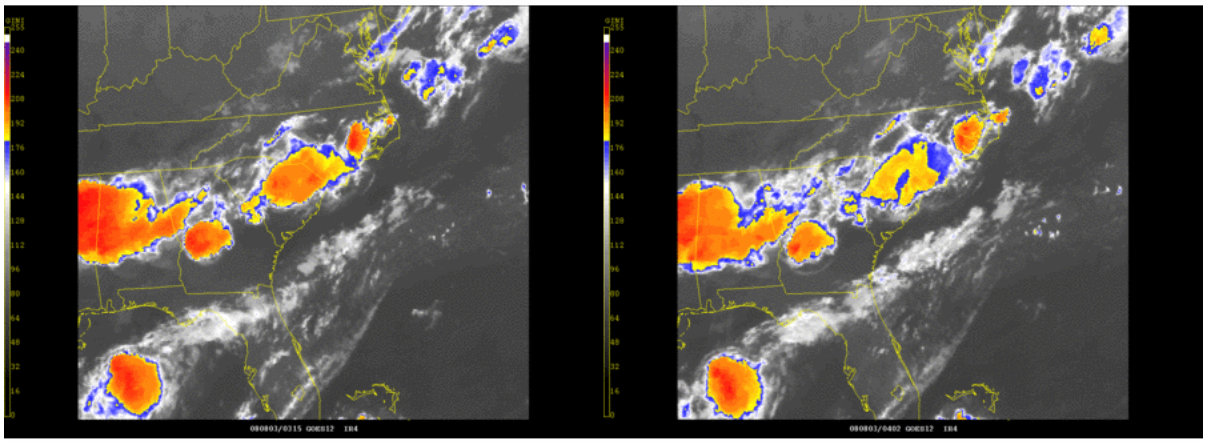

Aug 3, 2008 03Z

Aug 3, 2008 04Z

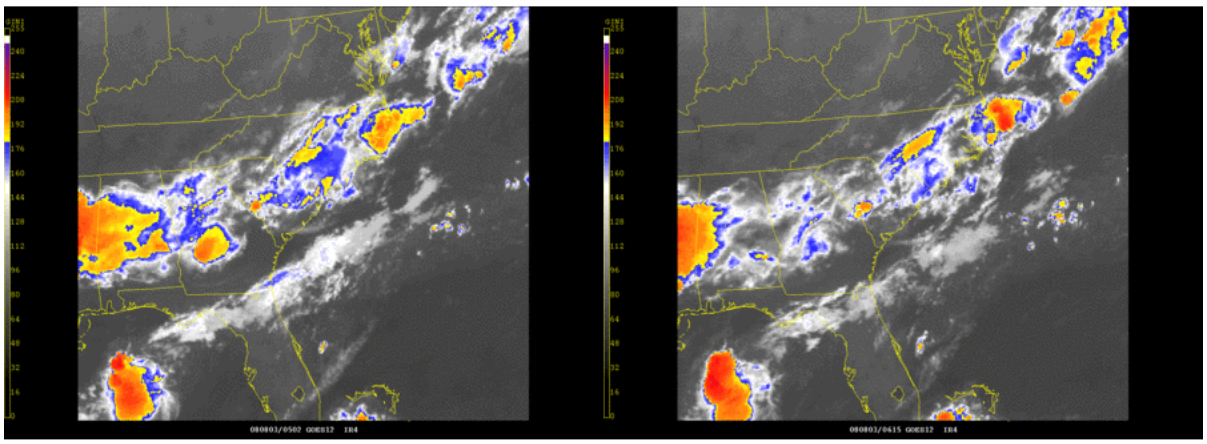

Aug 3, 2008 05Z

Aug 3, 2008 06Z

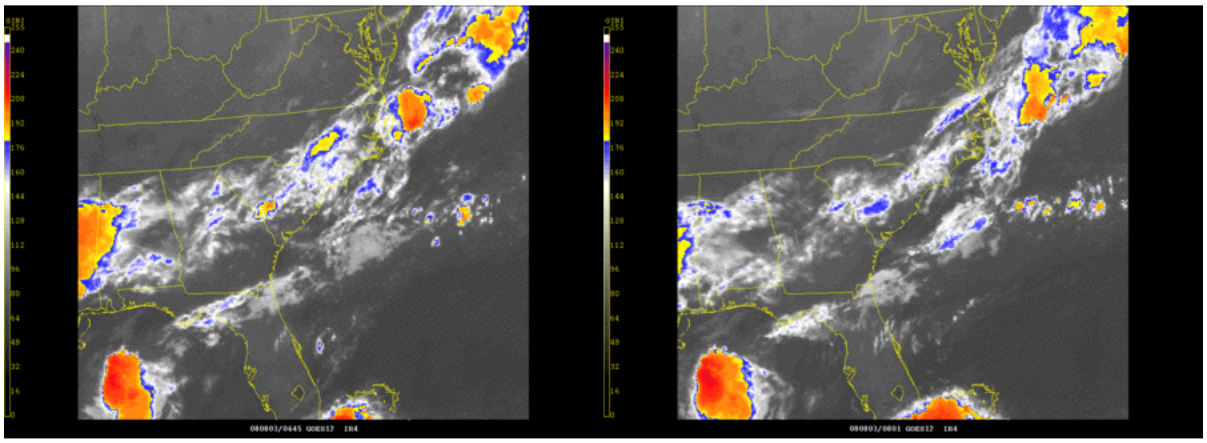

Aug 3, 2008 07Z

Aug 3, 2008 08Z

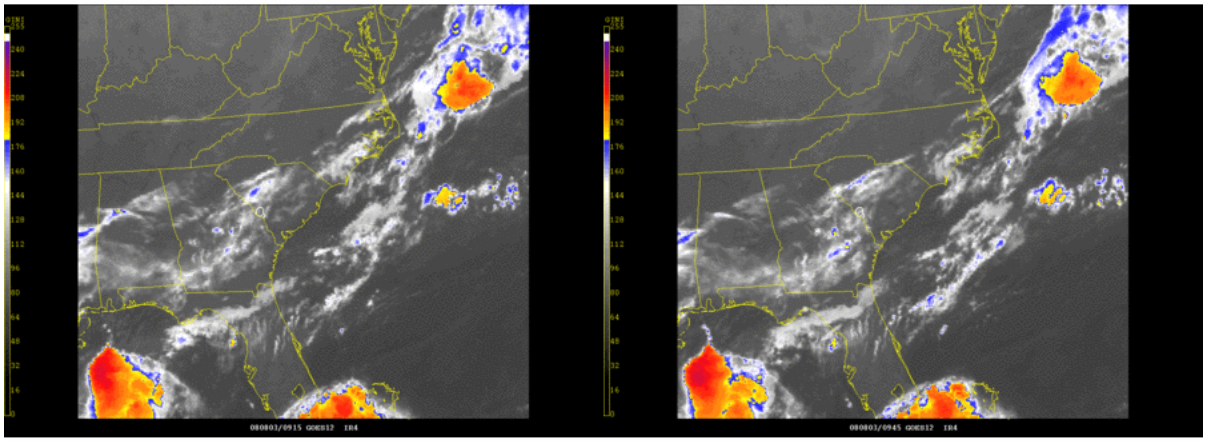

Aug 3, 2008 09Z

Aug 3, 2008 10Z

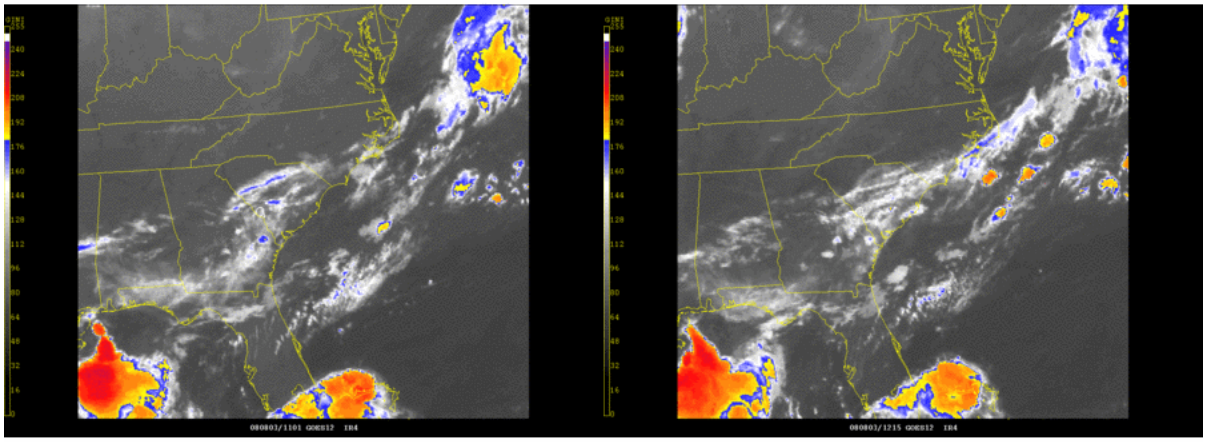

Aug 3, 2008 11Z

Aug 3, 2008 12Z

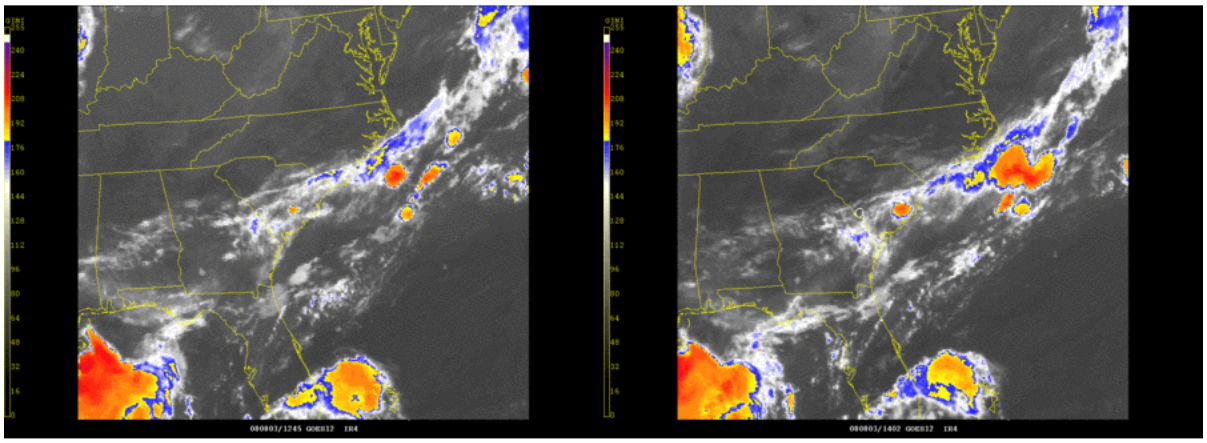

Aug 3, 2008 13Z

Aug 3, 2008 14Z

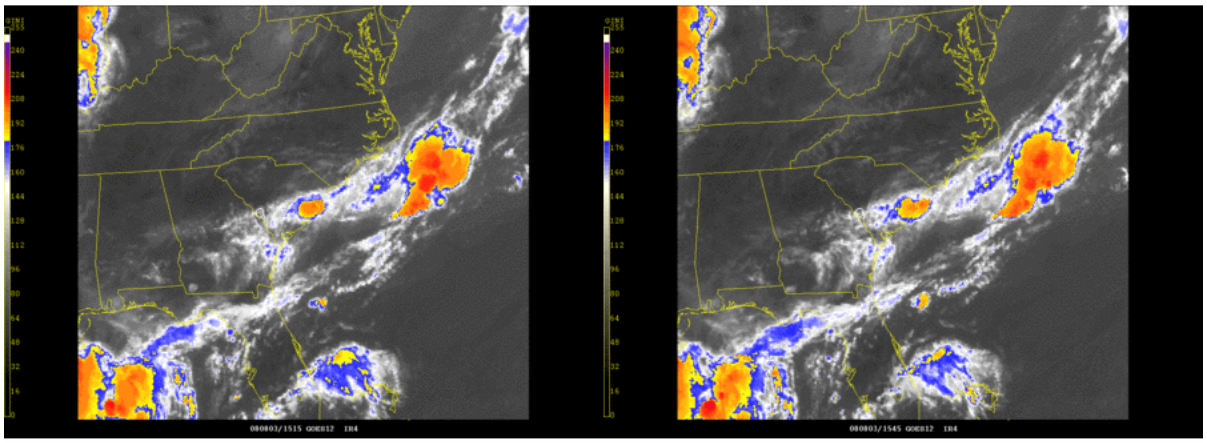

Aug 3, 2008 15Z

Aug 3, 2008 16Z

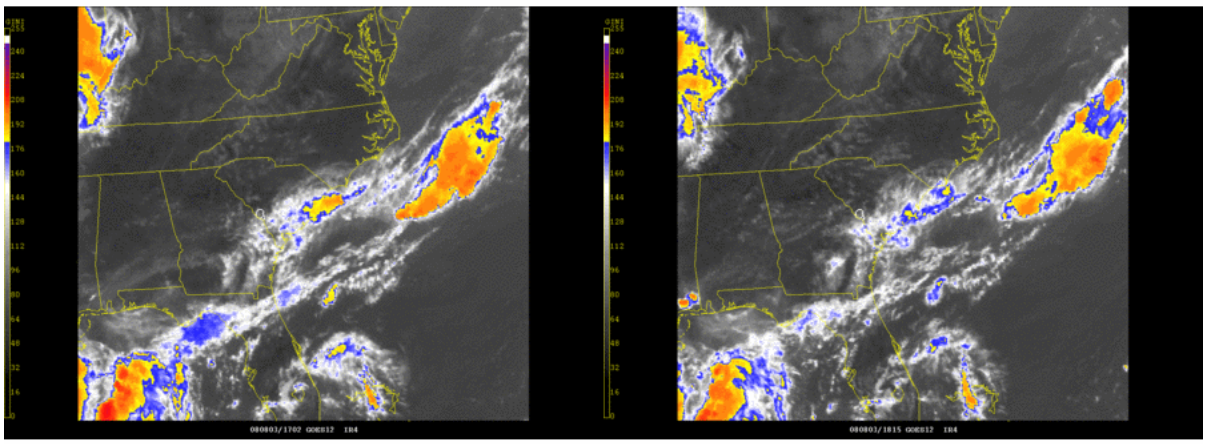

Aug 3, 2008 17Z

Aug 3, 2008 18Z

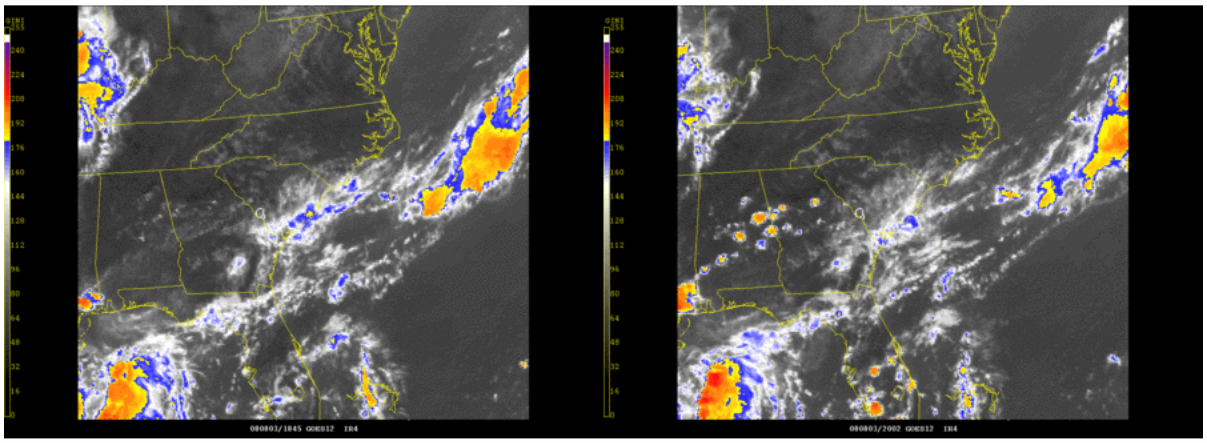

Aug 3, 2008 19Z

Aug 3, 2008 20Z

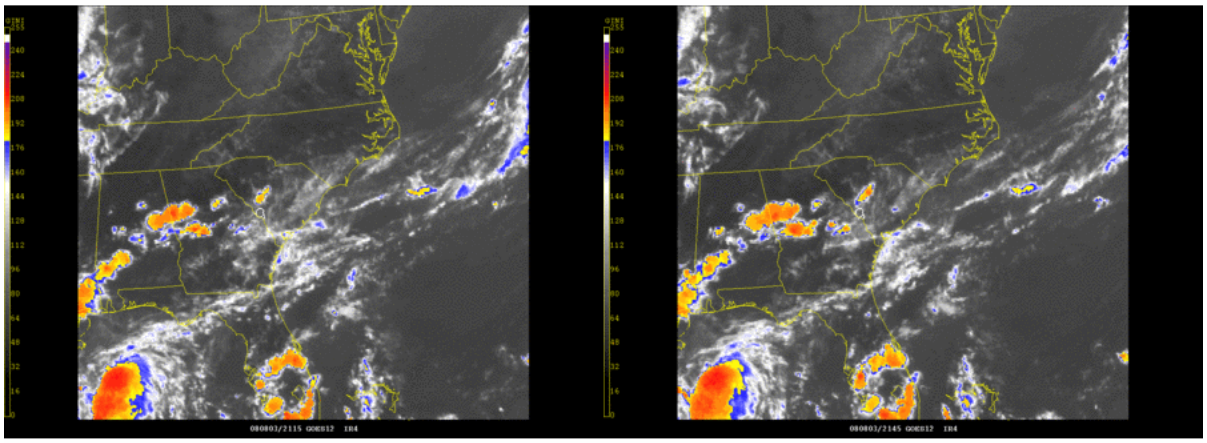

Aug 3, 2008 21Z

Aug 3, 2008 22Z

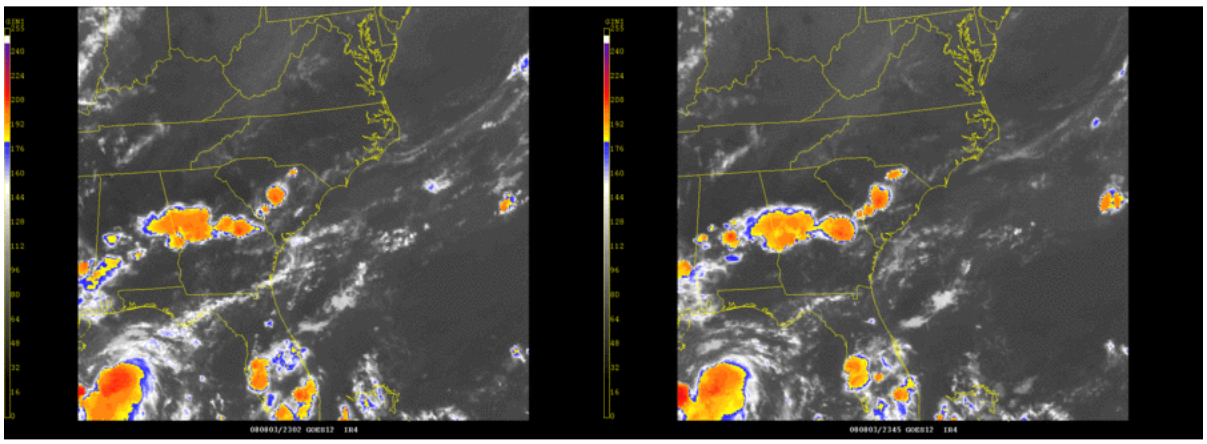

Aug 3, 2008 23Z

Aug 4, 2008 00Z

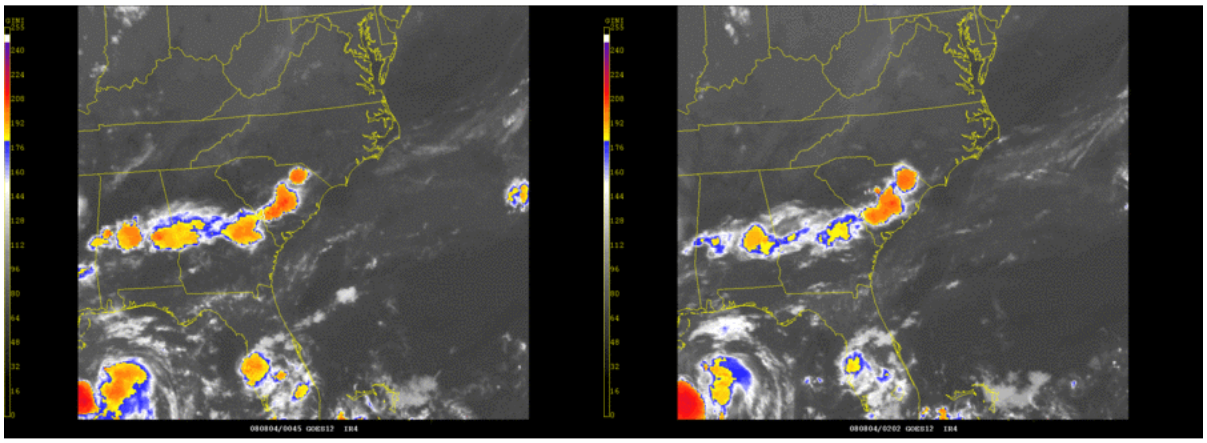

Aug 4, 2008 01Z

Aug 4, 2008 02Z

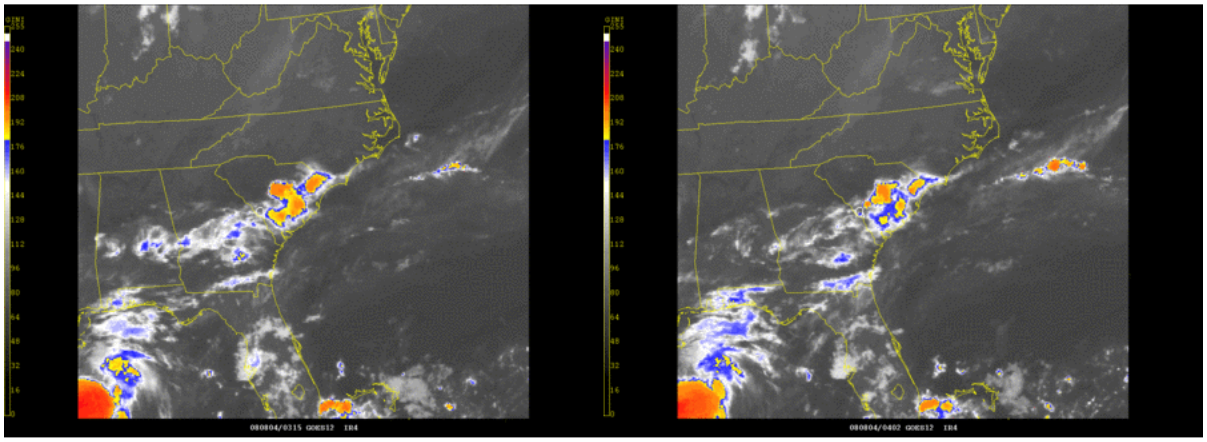

Aug 4, 2008 03Z

Aug 4, 2008 04Z

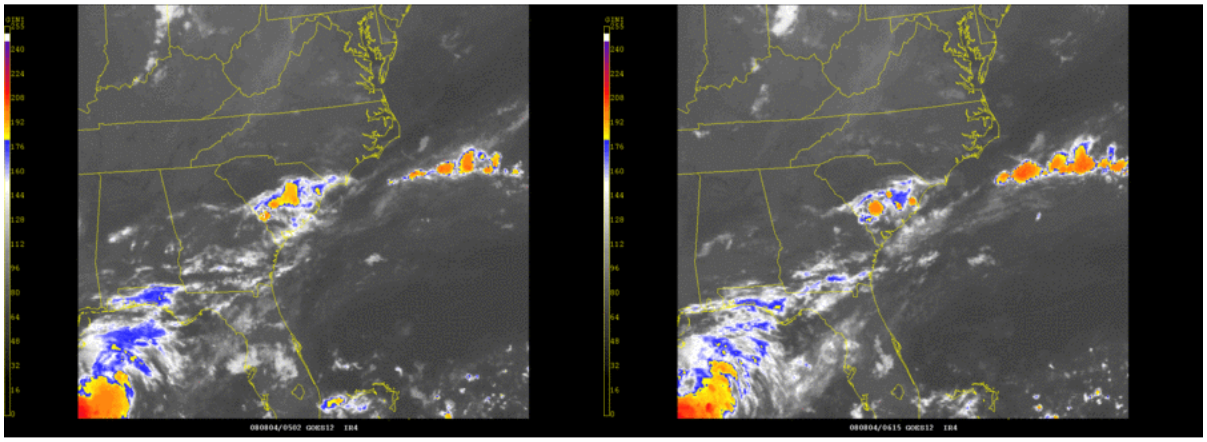

Aug 4, 2008 05Z

Aug 4, 2008 06Z

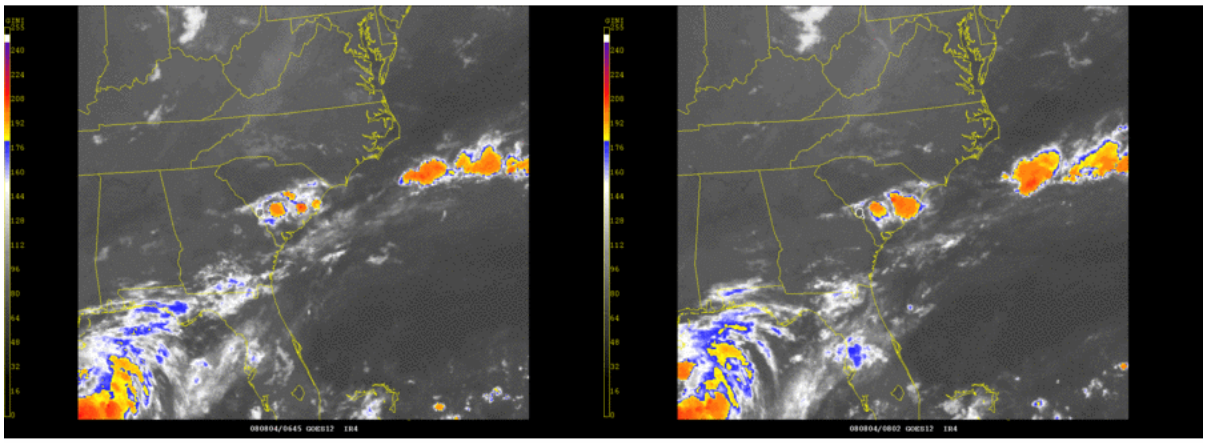

Aug 4, 2008 07Z

Aug 4, 2008 08Z

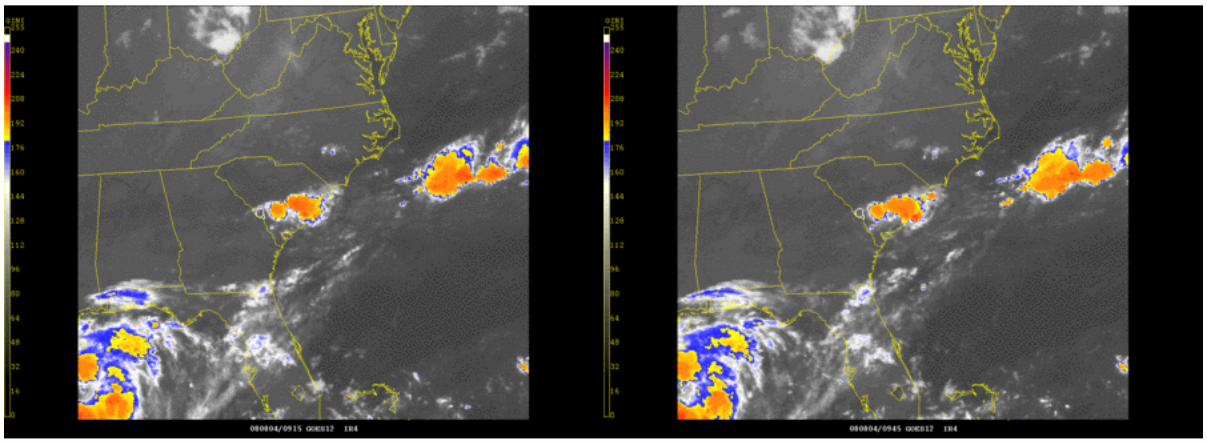

Aug 4, 2008 09Z

Aug 4, 2008 10Z

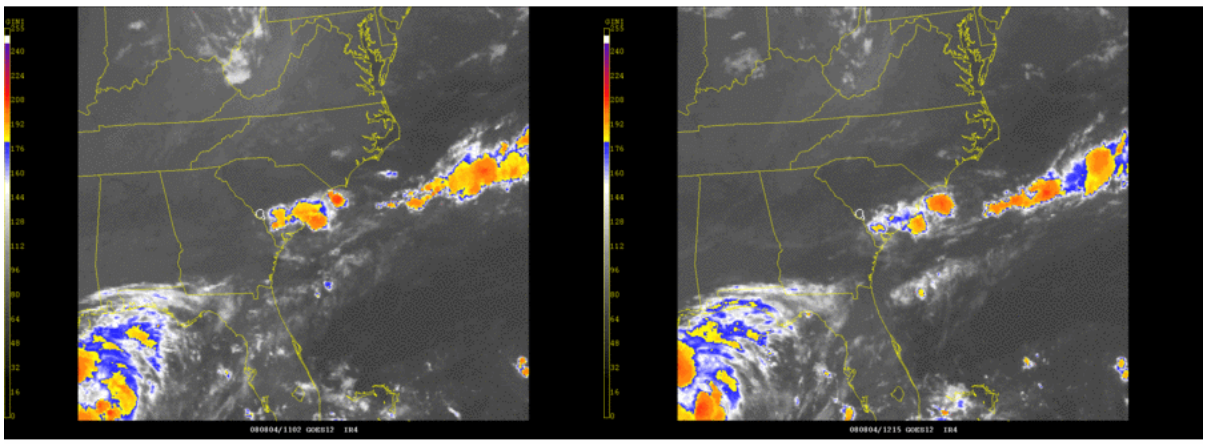

Aug 4, 2008 11Z

Aug 4, 2008 12Z

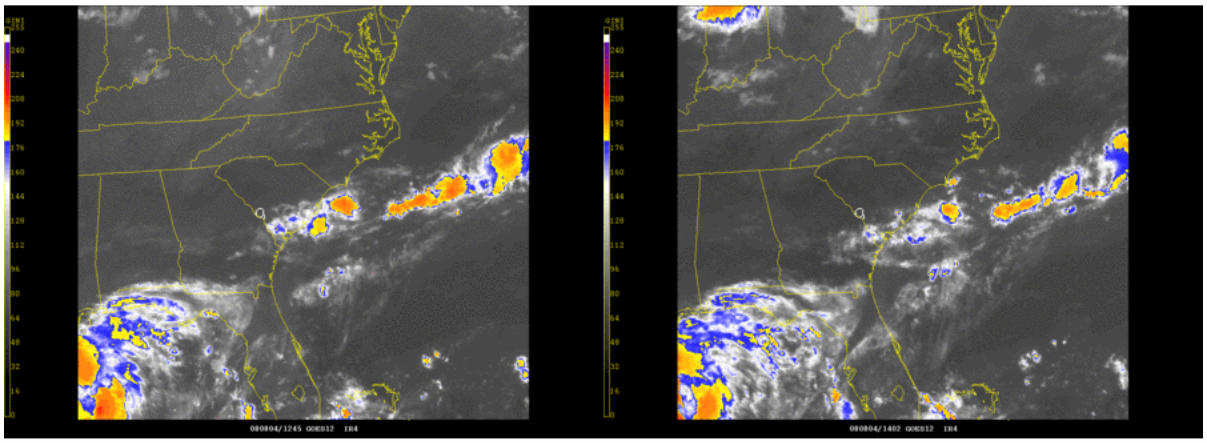

Aug 4, 2008 13Z

Aug 4, 2008 14Z

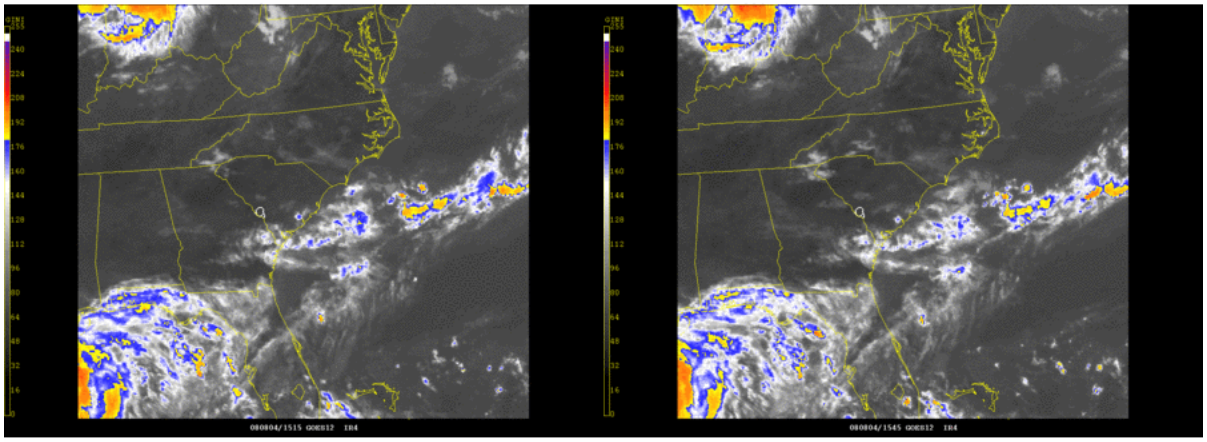

Aug 4, 2008 15Z

Aug 4, 2008 16Z

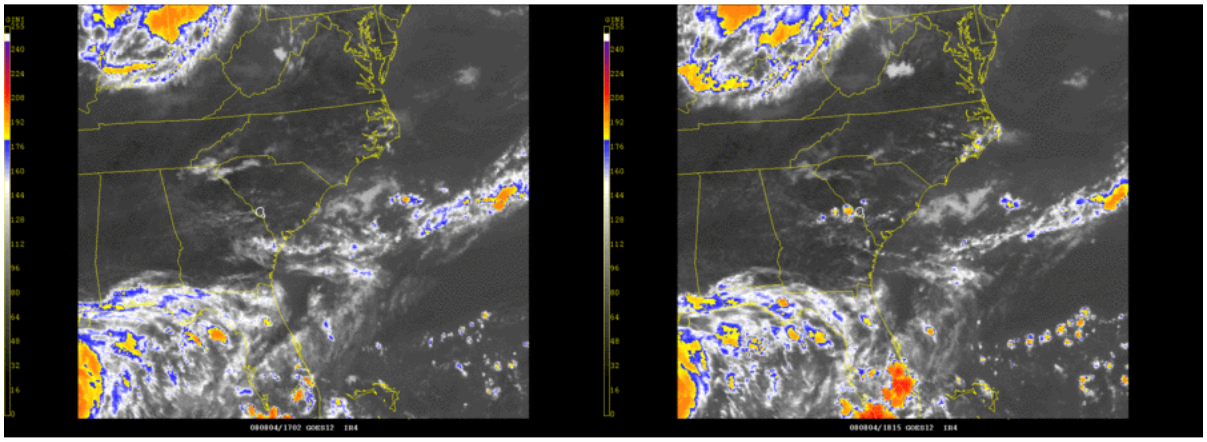

Aug 4, 2008 17Z

Aug 4, 2008 18Z

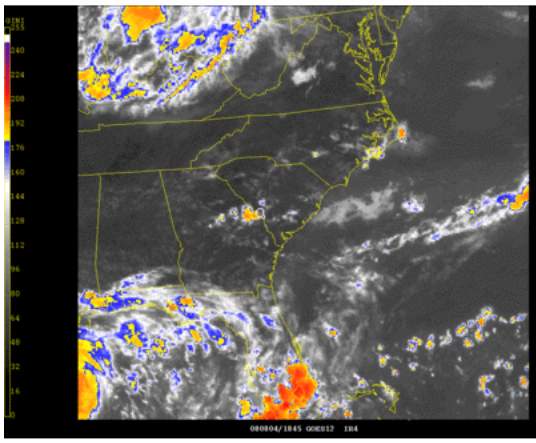

Aug 4, 2008 19Z

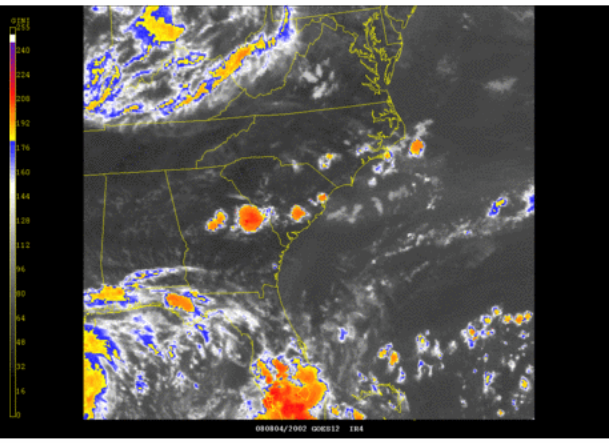

Aug 4, 2008 20Z

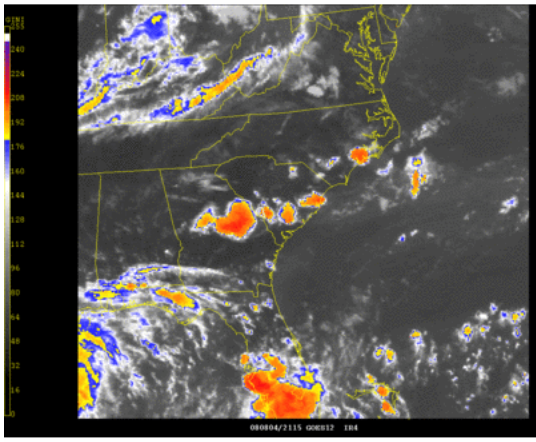

Aug 4, 2008 21Z

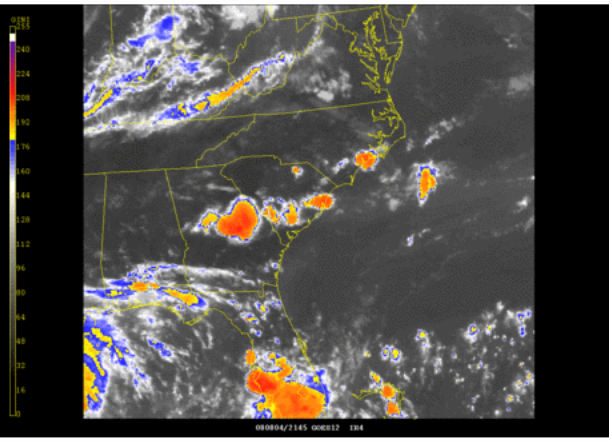

Aug 4, 2008 22Z

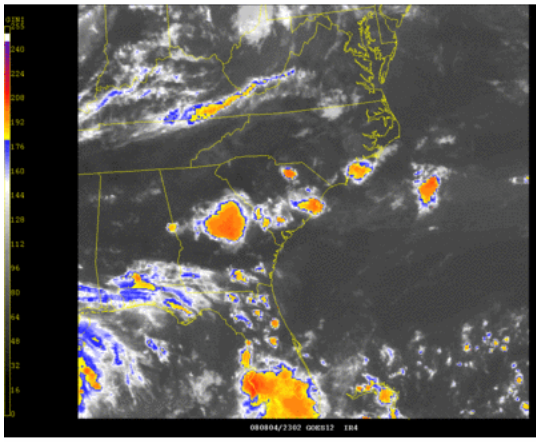

Aug 4, 2008 23Z

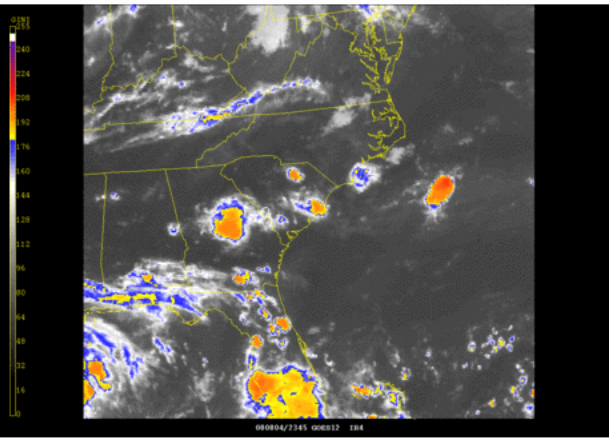

Aug 5, 2008 00Z

8.0 APPENDIX B. RADAR IMAGES 23:04-23:59 UTC AUGUST 03, 2008

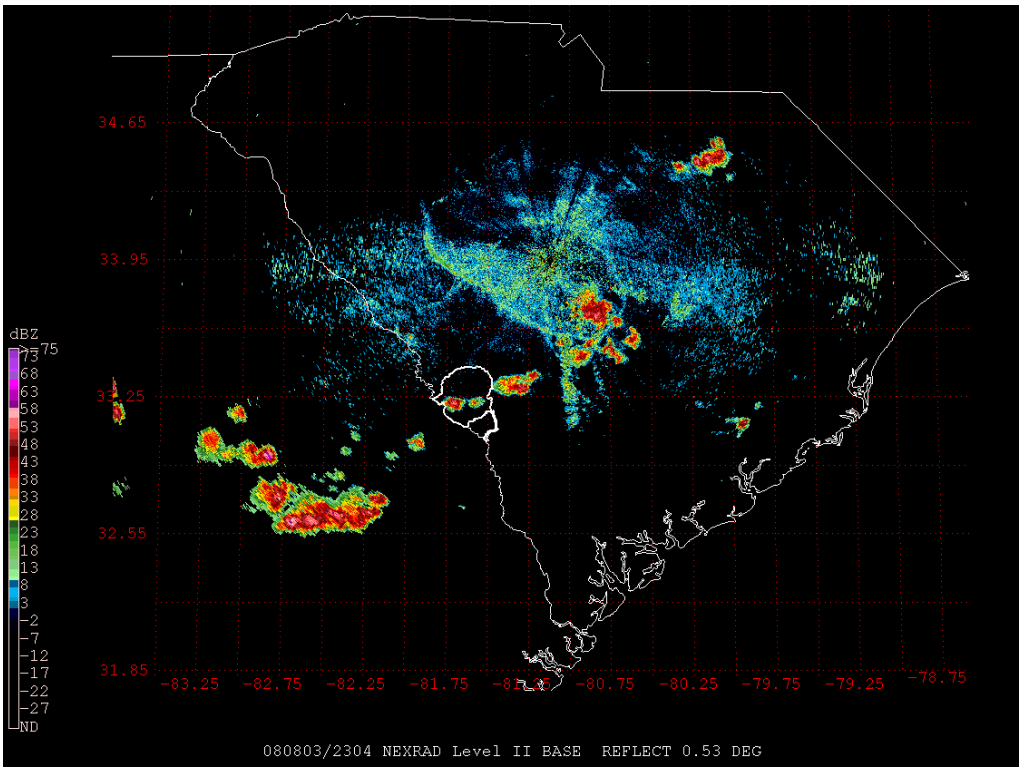

23:04 UTC Aug 3, 2008

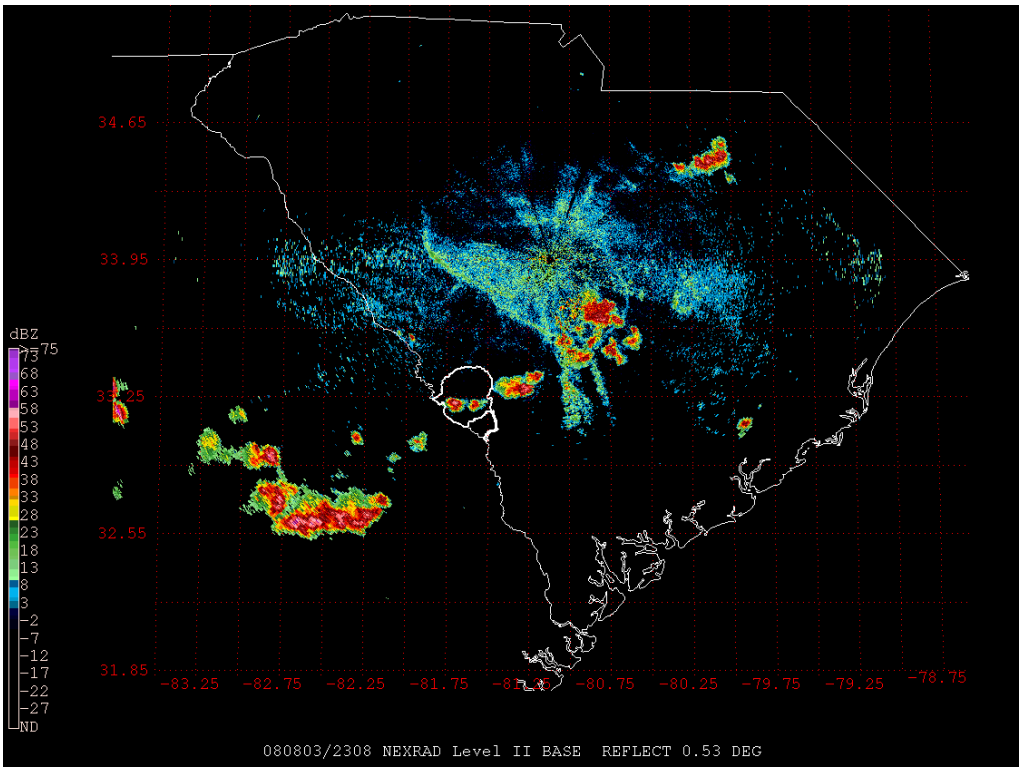

23:04 UTC Aug 3, 2008

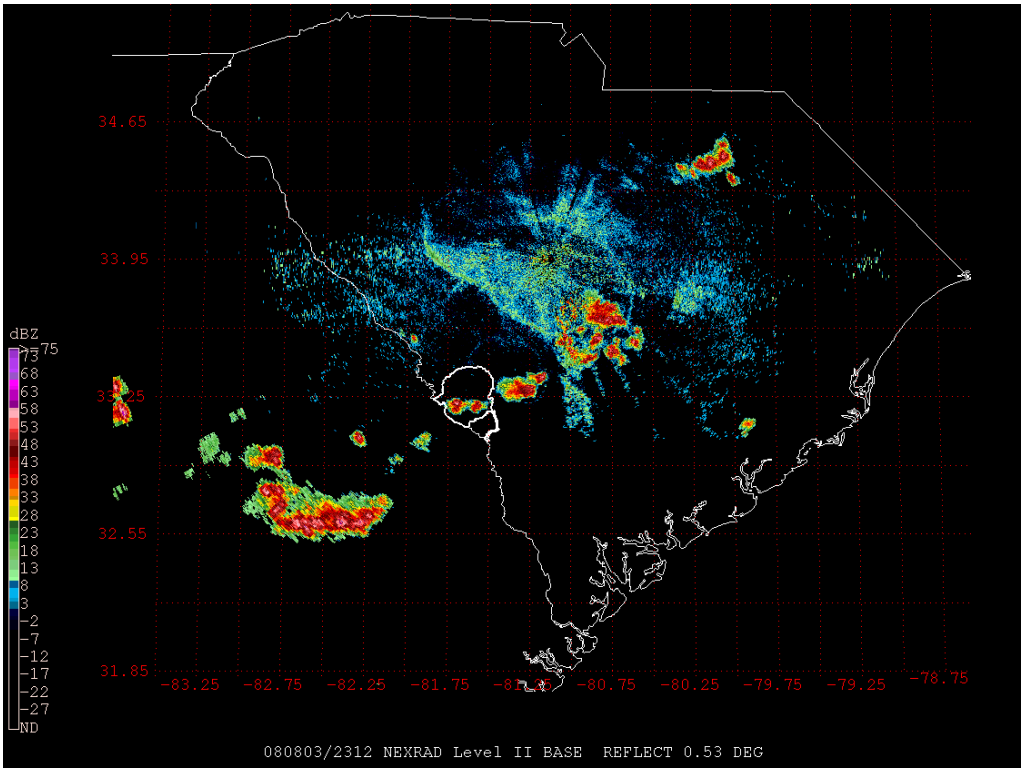

23:12 UTC Aug 3, 2008

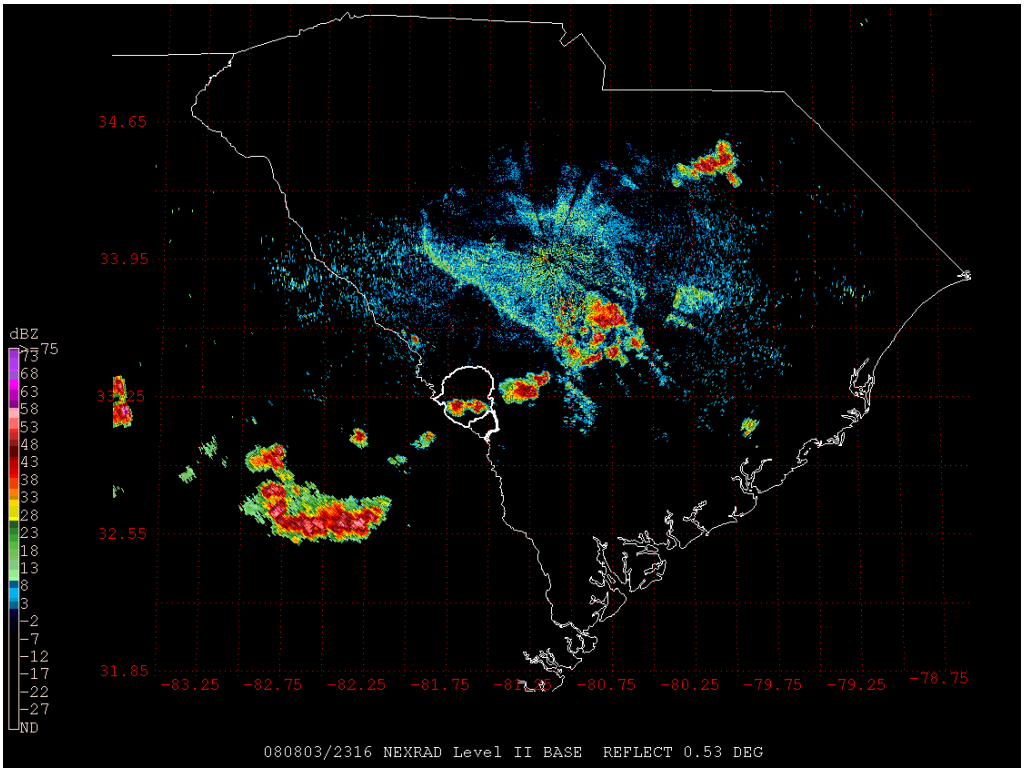

23:16 UTC Aug 3, 2008

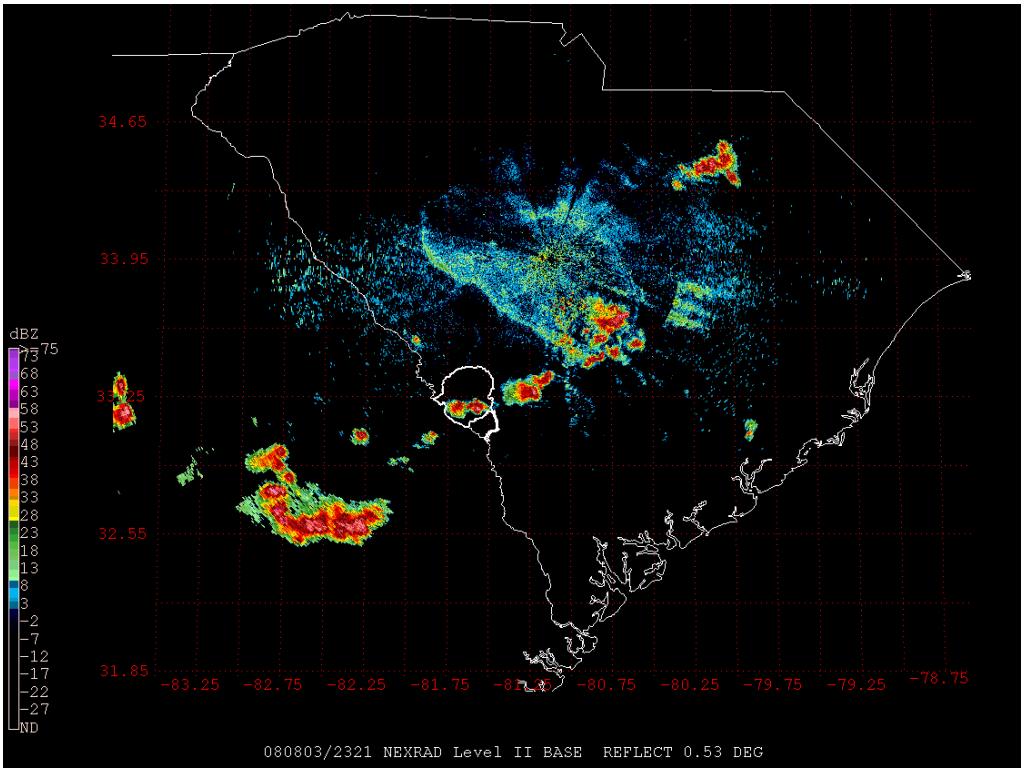

23:21 UTC Aug 3, 2008

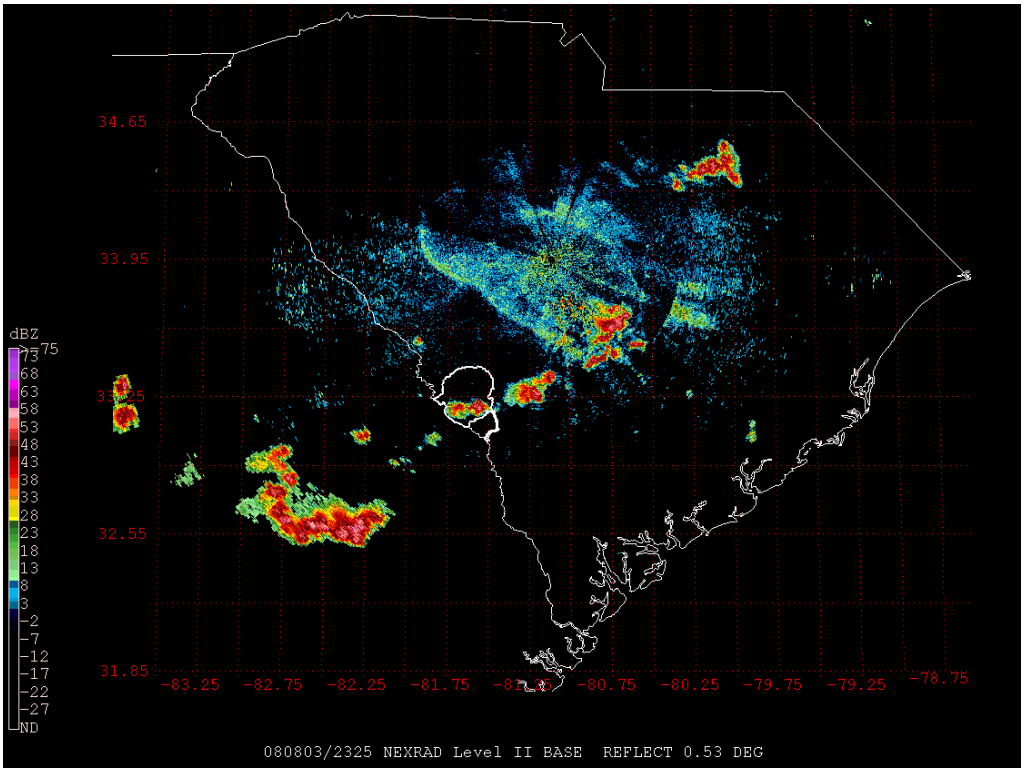

23:25 Aug 3, 2008

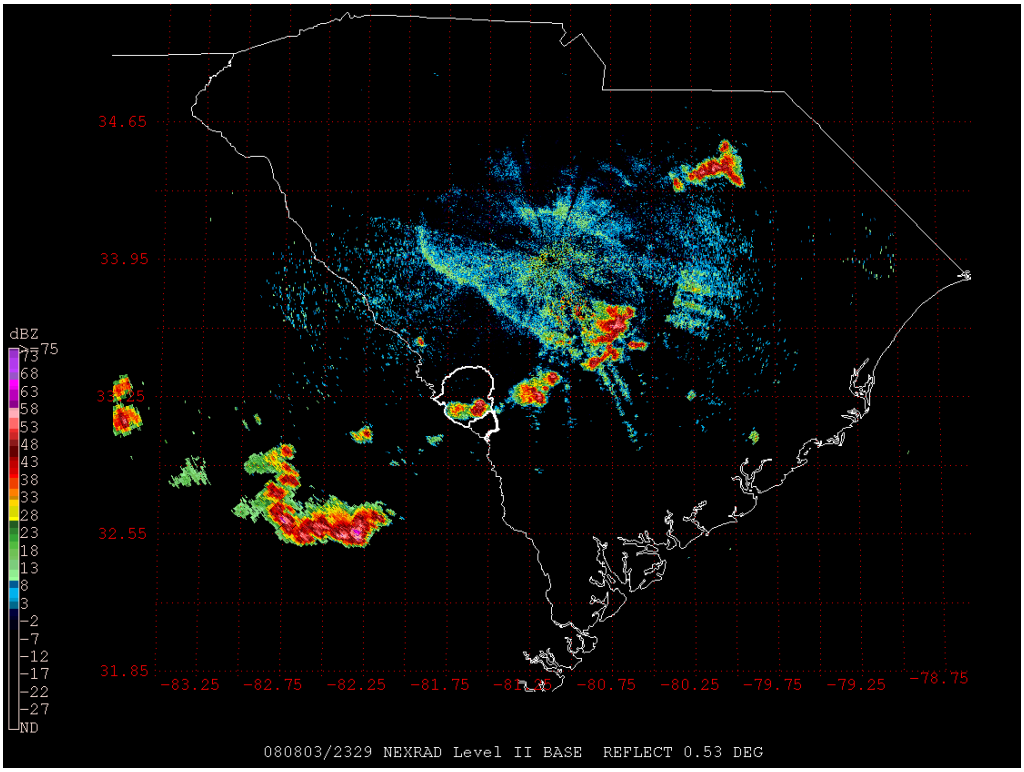

23:29 UTC Aug 3, 2008

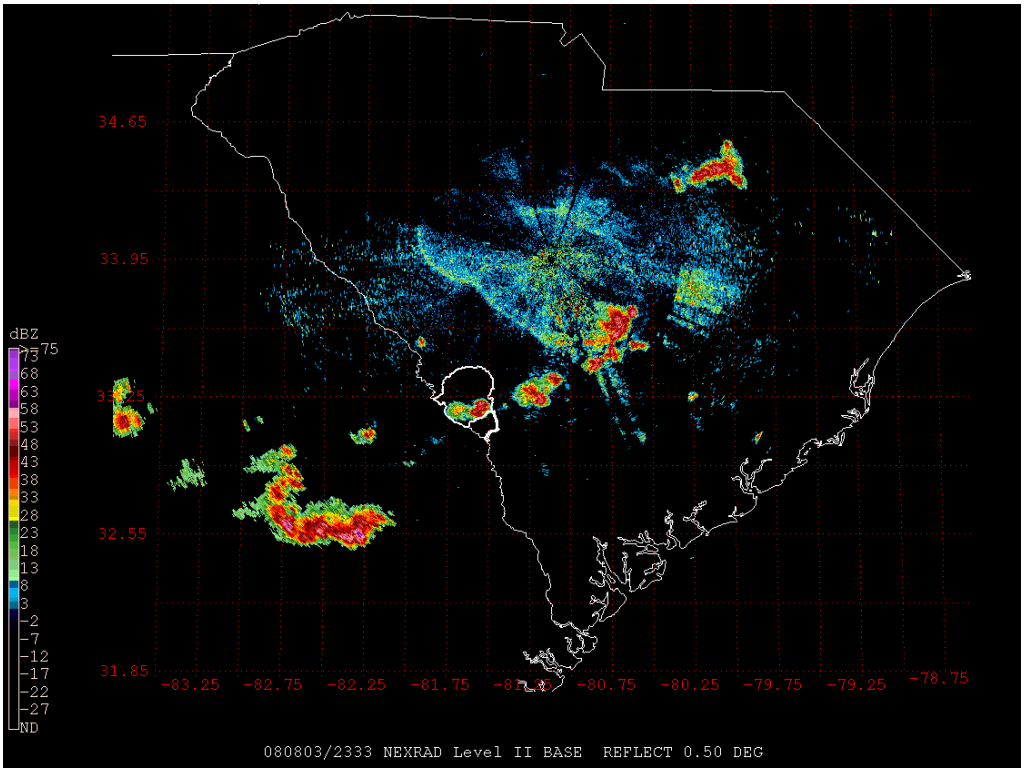

23:33 UTC Aug 3, 2008

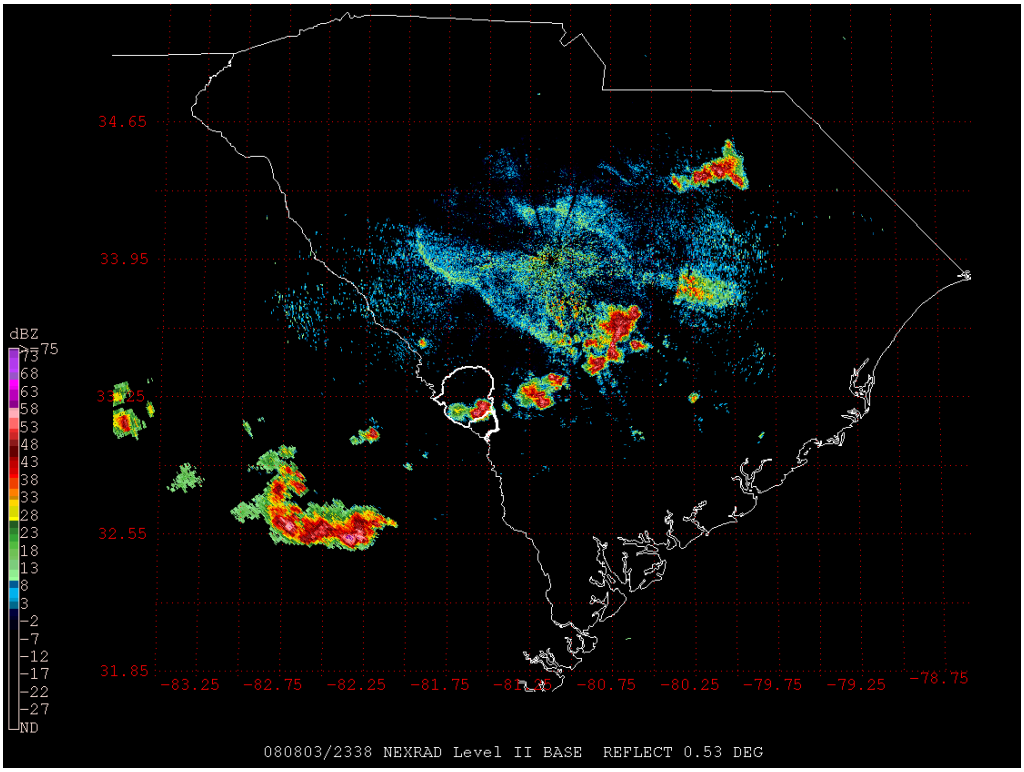

23:38 UTC Aug 3, 2008

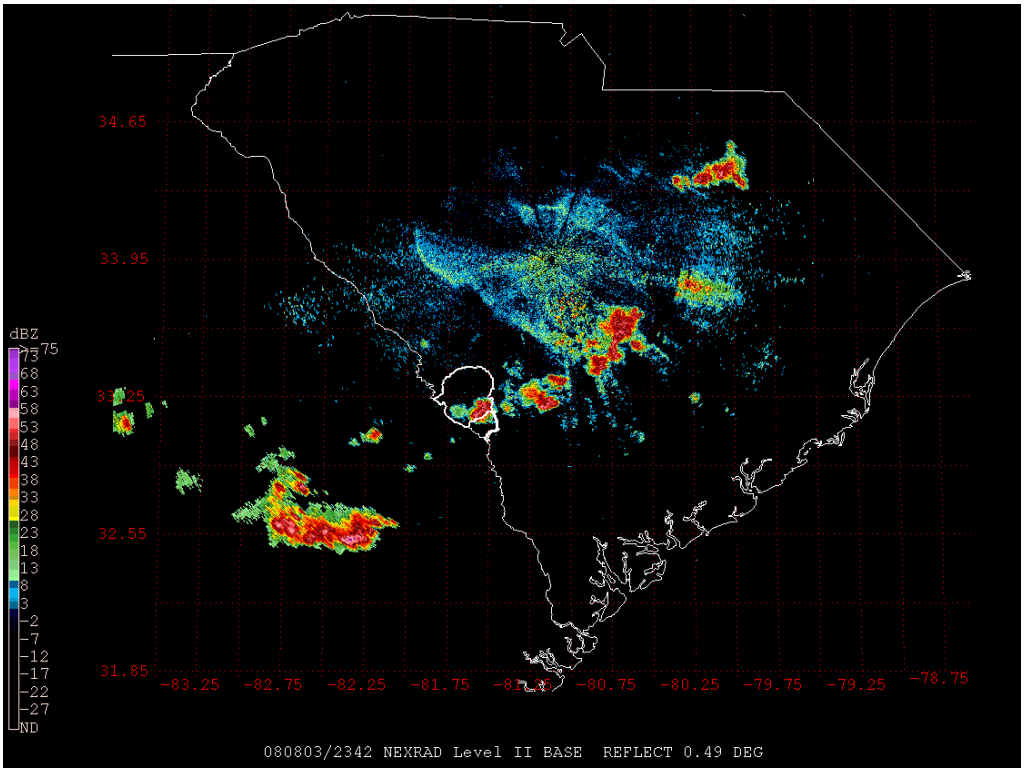

23:42 UTC Aug 3, 2008

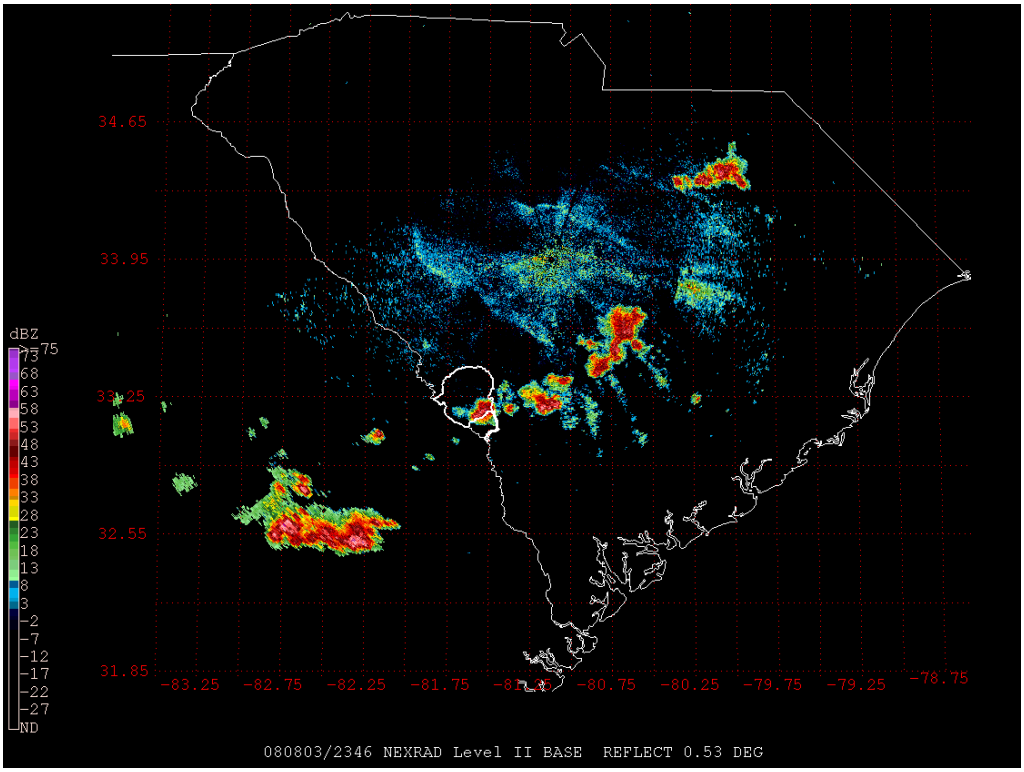

23:46 UTC Aug 3, 2008

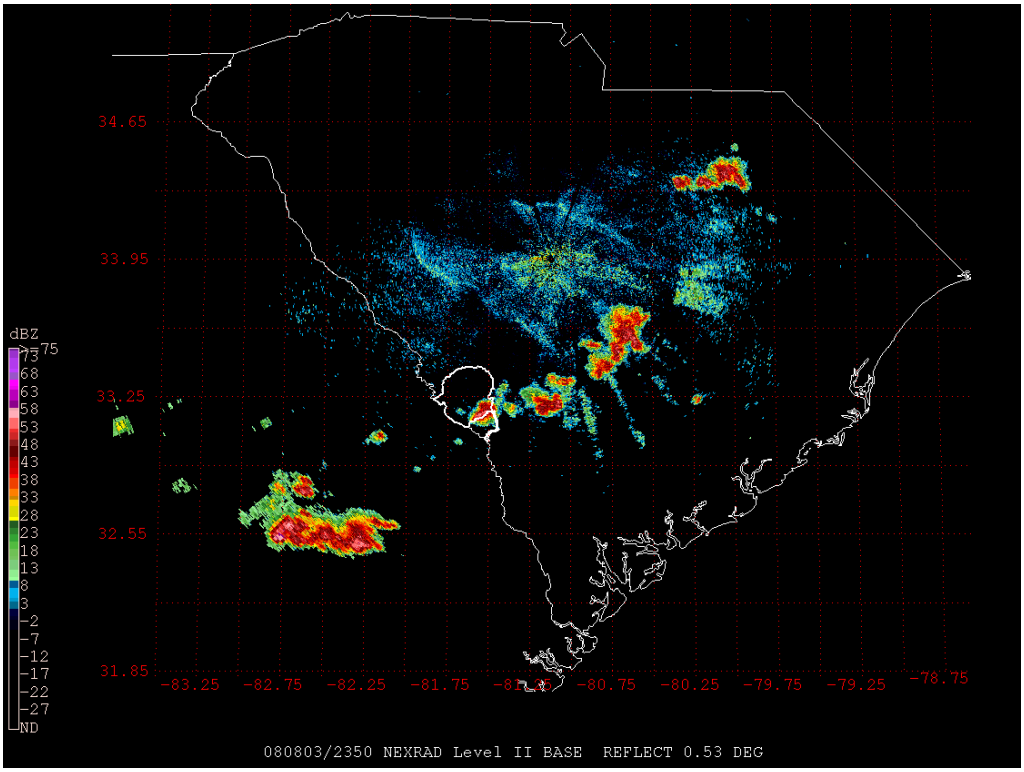

23:50 UTC Aug 3, 2008

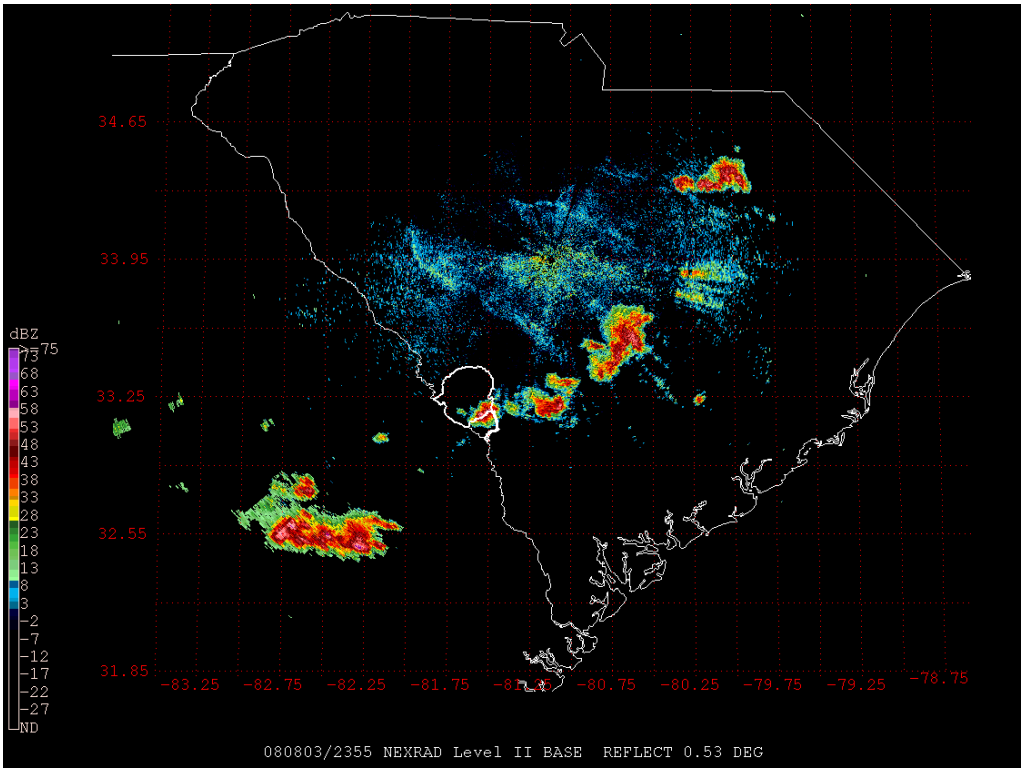

23:55 UTC Aug 3, 2008

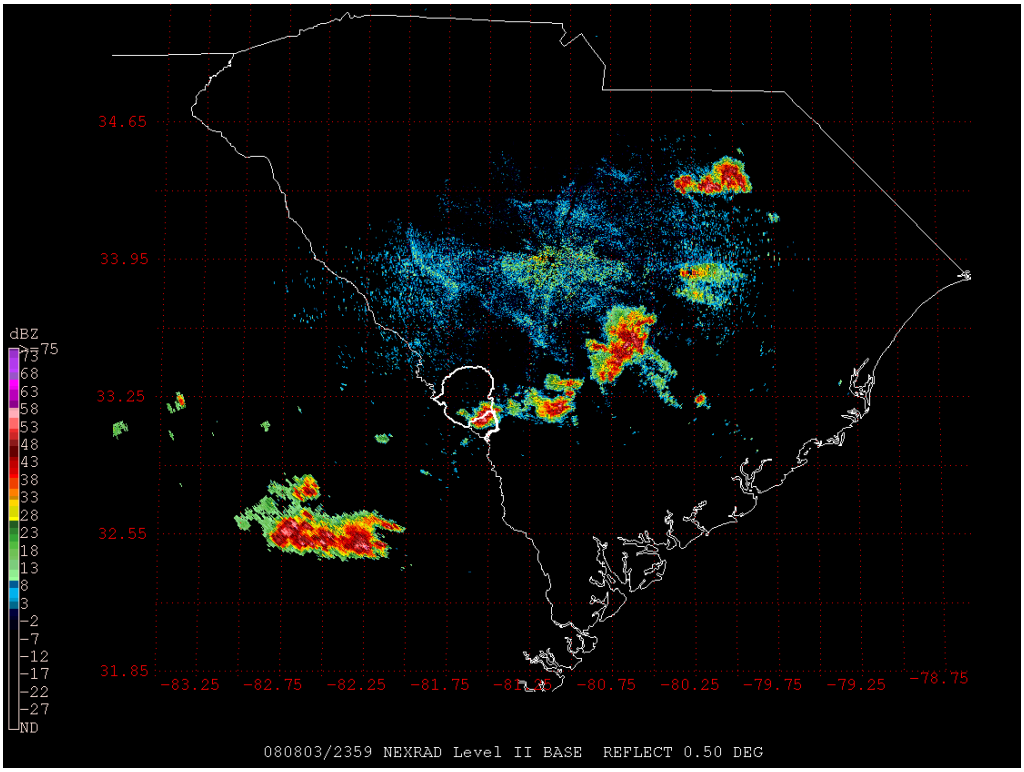

23:59 UTC Aug 3, 2008

9.0 APPENDIX C. LOCATIONS OF SRS METEOROLOGICAL TOWERS